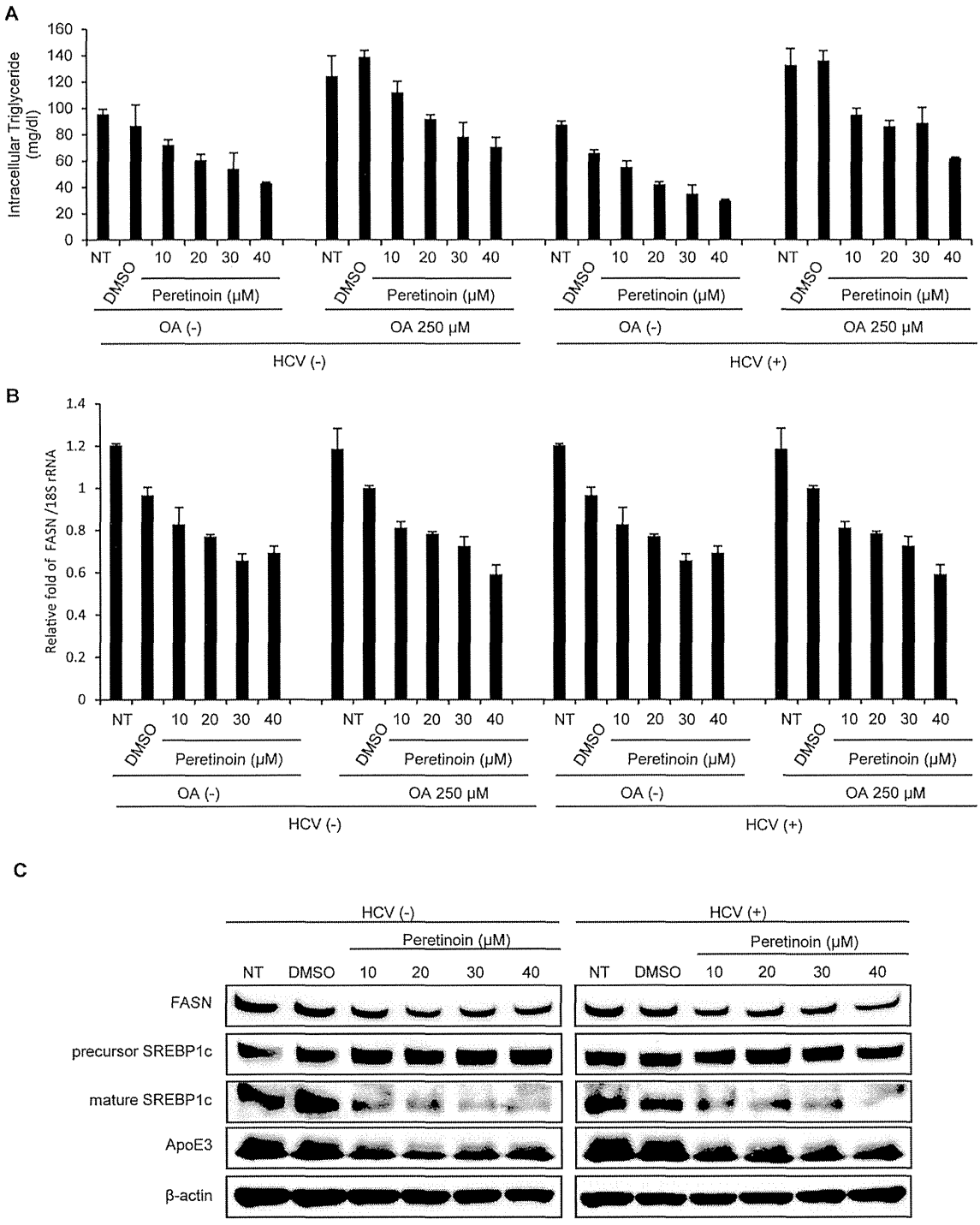

Figure 4 | Mechanism by which Peretinoin alters lipid metabolism. Huh-7.5 cells were transfected with H77S.3/GLuc2A RNA, and 72 h later, the transfected cells, depicted as 'HCV(+)', and non-transfected Huh-7.5 cells, depicted as 'HCV(-)', were treated with or without 250 μM OA in the presence of 2% fatty acid-free BSA with 0.5% DMSO or 10–40 μM Peretinoin, and the following assay was performed at 72 h later. (A) The concentration of intracellular TGs was measured. Data shown represent mean concentration ± SD from 3 independent experiments. (B) RNA was extracted and the levels of FASN mRNA and 18S rRNA were quantitated by RTD-PCR. FASN levels were normalised to those of 18S rRNA, and the ratio was furthermore normalised to that from DMSO-treated cells. The results presented here represent the relative fold of FASN/18S rRNA ± SD from 3 independent experiments at the indicated conditions. (C) Lysates from the cells without OA treatment were collected and subjected to western blot analysis using anti-FASN, anti-precursor SREBP1c, anti-mature SREBP1c, anti-ApoE3, and anti-β-actin antibodies. Full-length blots/gels are presented in Supplementary Fig. S7 online.

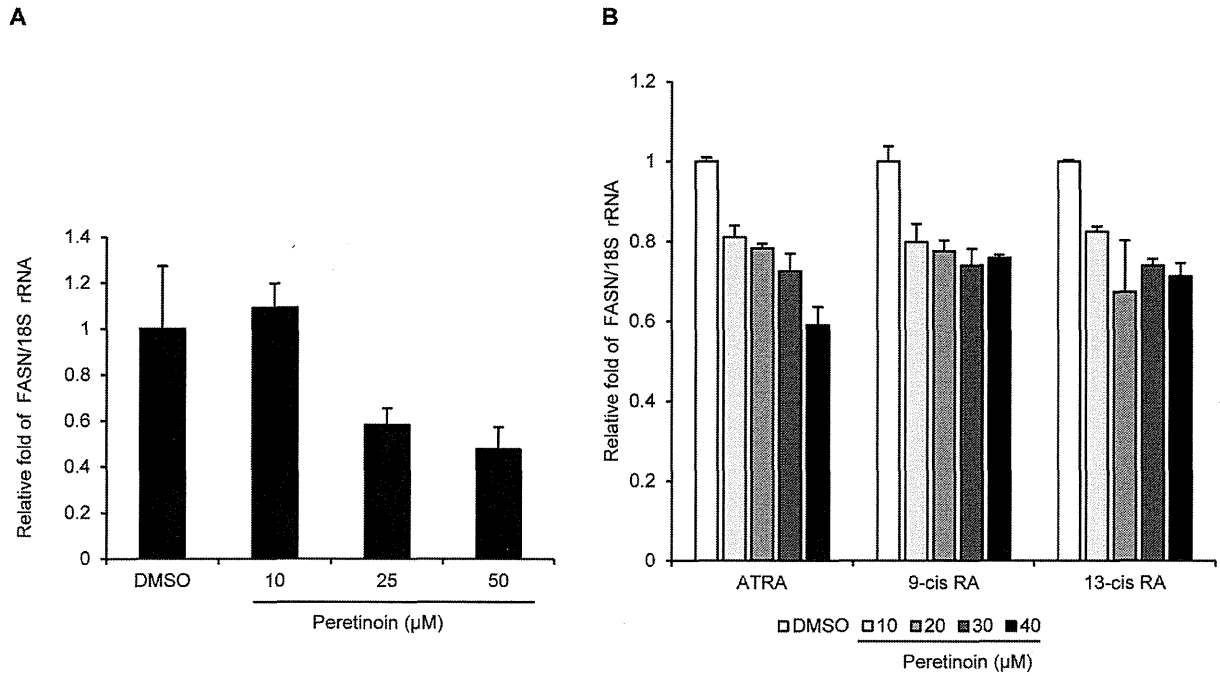

Figure 5 | Reduction of FASN mRNA levels by Peretinoin in a human hepatocyte cell line and the effects of ATRA, 9-cis RA, and 13-cis RA on the expression of FASN mRNA. (A) An immortalised human hepatocyte cell line, THLE-5b cells, was treated with the indicated concentrations of Peretinoin. At 72 h later, RNA was extracted and reverse transcribed, and the levels of FASN mRNA and 18S rRNA were quantified by RTD-PCR. The relative amount of FASN mRNA normalised to that of 18S rRNA is presented as fold change compared to DMSO-treated cells from 3 independent experiments at the indicated conditions. (B) Huh-7.5 cells were transfected with H77S.3/GLuc2A RNA. At 72 h later, the transfected cells were treated with DMSO or 10–40 μM ATRA, 9-cis RA, and 13-cis RA. At 72 h later, RNA was extracted and the levels of FASN mRNA and 18S rRNA were quantified by RTD-PCR. The relative amount of FASN mRNA was determined as described in Fig. 4 and presented as fold change compared to DMSO-treated cells from 3 independent experiments at the indicated conditions.

impaired virus secretion without affecting assembly at 10–30 μM, whilst 40 μM Peretinoin impaired virus secretion and assembly (Fig. 6A). The role of LDs in virus secretion has not been fully characterised, but virus should be secreted through the production and release of very low-density lipoproteins. In addition to microsomal triglyceride transfer protein and several apolipoproteins, such as ApoB and ApoE[23], small interfering RNA screening revealed that multiple components of the secretary pathway, including endoplasmic reticulum to Golgi trafficking and lipid and protein kinases, are involved in HCV secretion[24]. Thus, the mechanism underlying this specific inhibition of virus secretion by Peretinoin remains to be addressed. One possible explanation for its action is the reduction of ApoE3 expression (Fig. 4C), because ApoE3 was shown to have an important role in virus secretion with a minimal impact on assembly[25].

Several reports showed that LDs play an essential role in RNA amplification and virus assembly. The hypolipidemic agent nordihydroguaiaretic acid reduced the number of LDs, resulting in the suppression of RNA amplification and virus secretion, as Peretinoin did[26]. Furthermore, inhibition of tail-interacting protein 47, which coats LDs and is involved in their generation and turnover, suppressed HCV RNA replication and assembly[27,28]. Thus, the inhibition of RNA replication by Peretinoin could be explained by its direct effect on LDs. In addition, a recent report suggested that FASN may localise within HCV replication complexes through an interaction with NS5B, thereby increasing its RNA-dependent RNA polymerase activity[29]. Thus, Peretinoin may inhibit RNA replication not only by reducing the signalling of LDs but also inhibiting the expression of FASN.

We also demonstrated that Peretinoin reduced the levels of mature SREBP1c by inhibiting the proteolysis of its precursor, and subsequently the transcription and expression of FASN (Fig. 4C), which could be the main reason for the alteration of lipid metabolism by Peretinoin; however, the mechanism by which it inhibits proteolysis should be addressed in a future study. Several reports have shown that the expression of SREBP1c and/or FASN is increased in HCV-infected patients[30], Huh-7 cells[31], and a transgenic mouse expressing the full-length HCV polyprotein[32]. In addition, HCV infection was shown to enhance the proteolytic cleavage of precursor SREBP1c, resulting in an increase in its mature form[33]. Taken together, HCV induces lipogenesis to make infected cells more supportive for its propagation. In contrast to HCV, Peretinoin seems to suppress lipogenesis by inhibiting the SREBP1c-FASN axis, which is highly activated by HCV infection. It is also important to note that this effect did not depend on HCV infection, indicating that Peretinoin should exert a hypolipidemic effect, as we also observed a reduction of FASN mRNA levels following Peretinoin treatment of an immortalised human hepatocyte cell line (Fig. 5A). Interestingly, this effect was universal among retinoids because the other retinoids examined also reduced FASN mRNA levels (Fig. 5B). These findings suggest that Peretinoin could also be useful for the treatment of non-alcoholic fatty liver disease, whose hallmark is hepatic fat accumulation.

The antiviral EC_{50} of Peretinoin seems to be closer to its CC_{50} than that of the other retinoids in Huh-7.5 cells because several papers have shown that Peretinoin inhibits the growth of hepatoma cells *in vivo* and *in vitro*[34,35], induces apoptosis in human hepatoma cell lines[36], and causes an arrest of the cell cycle in G0-G1 in human hepatoma cell lines[35], indicating that Peretinoin should selectively

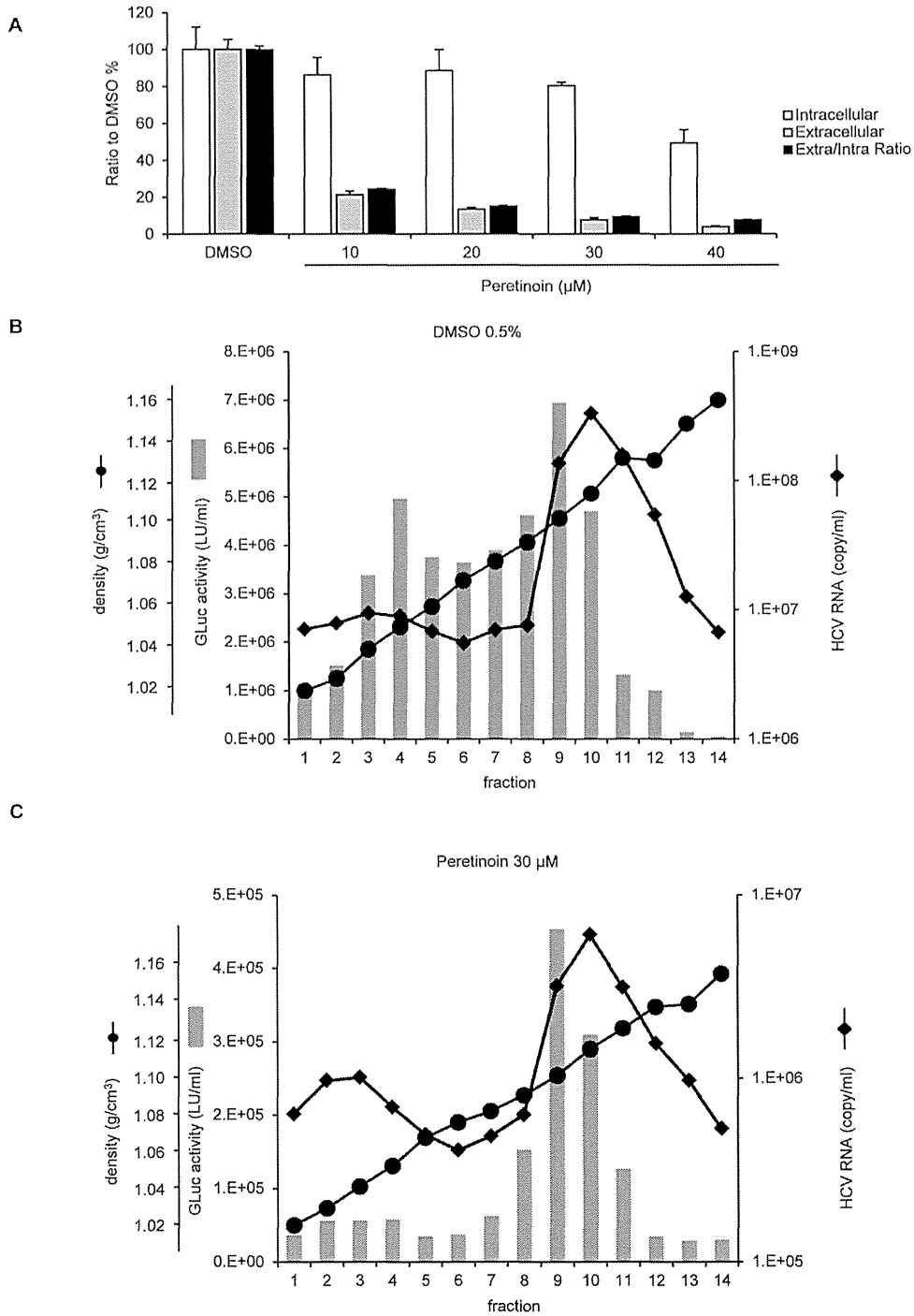

Figure 6 | Impact of Peretinoin on infectious virus production. (A) FT3-7 cells were transfected with HJ3-5/GLuc2A RNA, and 7 days later, 0.5% DMSO, or 10–40 μM Peretinoin, were added. At 72 h later, extra- and intra-cellular viruses were collected and used to infect naïve Huh-7.5 cells. Replication capacity was also determined by measuring secreted GLuc activity. At 48 h after infection, we determined the amount of infectious virus from extra- and intra-cellular media by using GLuc activity as an indicator of the amount of infectious virus. Intra- and extra-cellular infectivity was normalised to replication capacity at infection, and these were then normalised to those of DMSO-treated cells, which were set to 100%. The ratio of extracellular infectious virus to intracellular virus was calculated at the indicated conditions, and it was then normalised to DMSO-treated cells, which were set to 100%. Data show the mean ratio to that of DMSO-treated cells ± SD from 3 independent experiments. (B, C) FT3-7 cells were transfected with HJ3-5/GLuc2A RNA, and 7 days later, 0.5% DMSO or 30 μM Peretinoin were added, and then 72 h later, the medium was collected and subjected to equilibrium ultracentrifugation. Fourteen fractions were taken and analysed for density (circles), HCV RNA levels (diamonds), and infectious virus titres determined by GLuc activity (grey bars). (B) shows the results from DMSO-treated cells, whilst (C) shows those for Peretinoin-treated cells.

suppress the growth of hepatoma cells, although the mechanism has not been fully understood. However, pharmacokinetic data from humans showed that the mean plasma concentration of lipid-bounded Peretinoin is 7.3 μM when patients received 600 mg Peretinoin daily for 8 weeks[37]. This concentration is very close to the antiviral EC_{50} and could have an inhibitory effect on HCV replication, indicating that we could expect an antiviral effect at this dose in humans. Peretinoin showed an additive antiviral effect when combined with IFNα-2b (data not shown); furthermore, HCV did not acquire resistance to Peretinoin after 14 days treatment with 10–40 μM Peretinoin (see Supplementary Fig. S11 online). Although it could be difficult to eradicate HCV only by Peretinoin due to its low selective index (CC50/EC50), combination therapy with Peretinoin plus PEG-IFN, ribavirin, or DAAs may further improve the SVR rate, as vitamin D has been proved to do[38,39].

In summary, we have demonstrated that Peretinoin, which may in the future be administered to patients infected with HCV to prevent HCC, inhibits HCV RNA replication and infectious virus release by modifying several aspects of lipid metabolism.

Methods

Cell lines. Huh-7.5 (kindly provided by Professor C. M. Rice, Rockefeller University, New York, NY), and FT3-7 cells (both clonal derivatives of Huh-7 cells) were maintained as described previously[9]. We used an immortalised human hepatocyte cell line, THLE-5b cells[40], for the indicated experiments.

Reagents. Peretinoin and IFNα-2b were kindly provided by KOWA Company, Ltd. (Tokyo, Japan). ATRA, 9-cis RA, and 13-cis RA, were purchased from Sigma-Aldrich Japan K.K. (Tokyo, Japan). Stock solutions were prepared in DMSO, and all final dilutions contained 0.5% DMSO.

Plasmids. The GLuc coding sequence, followed by the FMDV2A sequence, was inserted between p7 and NS2 in pJFH1 and pHCV-N.2, which encode cDNA of genotype 2a JFH1[13] and genotype 1b N[12], carrying several replication-enhancing mutations to be described elsewhere, respectively, by the same strategy adopted previously for H77S[10]. pH77S.3/GLuc2A[10], pHJ3-5/GLuc2A[9], and pHJ3-5[11] have been described previously.

Antiviral activity assay. The indicated HCV RNAs were transfected by electroporation. The medium was replaced with fresh medium containing serial dilutions of the antiviral compounds at 48 h, and at 24 h intervals thereafter. Secreted GLuc activity was determined at 72 h after adding the antiviral compounds. The concentration of each compound required to reduce the amount of secreted GLuc activity by 50% (EC_{50}) was determined using a 3-parameter Hill equation (Sigma Plot 10.0).

Cell number determination. Huh-7.5 cells were seeded in 96-well plates at a density of 5,000 cells/well, and at 24 h later, the indicated compounds were added. Cell numbers were determined by a WST-8 assay using Cell Counting Kit-8. The concentration of each compound required to reduce the amount of cell number by 50% (CC_{50}) was determined using a 3-parameter Hill equation (Sigma Plot 10.0).

RNA transcription. HCV RNAs were synthesised using a MEGAscript T7 Kit, and synthesised RNA was purified using an RNeasy Mini Kit.

Virus yield determination. Huh-7.5 cells were seeded in 48-well plates at a density of 4.0×10^4 cells/well at 24 h prior to inoculation with 100 μL of virus-containing medium. The cells were maintained at 37°C in a 5% CO_2 environment and fed with 300 μL medium at 24 h later. Following 48 h of additional incubation, the cells were fixed in methanol-acetone (1 : 1) at room temperature for 9 min and stained with a C7-50 monoclonal antibody to the HCV core protein (1 : 300). After extensive washing, the cells were stained with Alexa Fluor 568-conjugated anti-mouse IgG antibodies. A cluster of infected cells staining for core antigen was considered to constitute a single infectious FFU; virus titres are reported as FFUs/mL.

Western blotting and immunostaining. Western blotting and immunostaining were performed as described previously[41,42]. Briefly, the cells were washed in phosphate-buffered saline (PBS) and lysed in a radioimmunoprecipitation assay buffer containing complete Protease Inhibitor Cocktail and PhosSTOP. The membranes were blocked in Blocking One or Blocking One-P solution, and the expression of HCV core protein, FASN, precursor and mature SREBP1c, ApoE3, and β-actin was evaluated with mouse anti-core protein, rabbit anti-FASN, rabbit anti-SREBP1c, goat anti-ApoE3, and rabbit anti-β-actin antibodies, respectively.

For immunofluorescence staining, the cells were washed twice with PBS and fixed in 4% paraformaldehyde for 15 min at room temperature. After washing again with PBS, the cells were permeabilised with 0.05% Triton X-100 in PBS for 15 min at room temperature. They were incubated in a blocking solution (10% foetal bovine serum and 5% bovine serum albumin [BSA] in PBS) for 30 min, and then with the anti-core protein monoclonal antibodies. The fluorescent secondary antibodies were Alexa Fluor 568-conjugated anti-mouse IgG antibodies. Nuclei were labelled with DAPI, and LDs were visualised with BODIPY 493/503. Imaging was performed on a BIOREVO fluorescence microscope (Keyence Corporation, Osaka, Japan). The signal strength of LDs, core protein, and nuclei was quantitated by using Measurement Module BZ-H1M (Keyence Corporation).

Quantitative RTD-PCR. The primer pairs and probes for FASN and 18S rRNA were obtained from the TaqMan assay reagents library. HCV RNA was detected as described previously[43].

Secreted luciferase assay. Cell culture supernatant fluids were collected at intervals after RNA transfection and the cells were re-fed fresh medium. Secreted GLuc was measured as described previously[9].

Fatty acid treatment and measurement of TGs. The cells were treated with the indicated concentrations of OA in the presence of 2% fatty acid-free BSA. Intracellular TG content was measured using a TG Test according to the manufacturer's instructions.

Intra- and extra-cellular infectivity assay. To determine the amount of intra-cellular infectious virus, cell pellets of HJ3-5/GLuc2A-replicating FT3-7 cells harvested after trypsinization were resuspended in complete medium, washed twice with PBS, and lysed by 4 cycles of freezing and thawing. The lysates were clarified by centrifugation at 2,300 × *g* for 5 min prior to inoculation onto naïve Huh-7.5 cells. At the same time, extra-cellular medium was also collected. The medium derived from extra- and intra-cellular cultures was used to infect naïve Huh-7.5 cells, which were plated in 48-well plates at a density of 4.0×10^4 cells/well at 24 h prior to infection. After 6 h inoculation, medium containing virus and possible carryover of Peretinoin was removed by extensive wash, and medium was replaced with fresh one every 24 h until 48 h. At 48 h after infection, we determined GLuc activity and used it as an indicator of the infectious virus titre.

Equilibrium ultracentrifugation of HJ3-5/GLuc2A virus particles using an isopycnic iodixanol gradient. Filtered supernatant fluids collected from HJ3-5/GLuc2A virus-replicating FT3-7 cells treated with DMSO or 30 μM Peretinoin for 72 h were concentrated 30-fold using a Centricon PBHK Centrifugal Plus-20 Filter Unit with an Ultracel-PL membrane (100-kDa exclusion; Merck Millipore, Billerica, MA), then layered on top of a preformed continuous 10–40% iodixanol gradient in Hanks' balanced salt solution. The gradients were centrifuged in an SW41 rotor at 209,678 × *g* for 16 h at 4°C, and fractions (500 μL each) were collected from the top of the tube. The density of each fraction was determined using a digital refractometer. Virus RNA was isolated from each gradient fraction using a QIAamp Viral RNA Kit, and cDNA was synthesised using a High Capacity cDNA Reverse Transcription Kit. RTD-PCR to quantitate the amount of HCV RNA was performed using a 7500 Real Time PCR System. Each fraction was used to infect naïve Huh-7.5 cells for 6 h, followed by extensive washing to ensure GLuc activity was reduced to background. The infected cells were inoculated and the medium was replaced with fresh medium every 24 h. GLuc activity, which was used an alternative to the infectious virus titre, was determined at 72 h after infection.

1. Fried, M. W. *et al.* Peginterferon alfa-2a plus ribavirin for chronic hepatitis C virus infection. *N Engl J Med* **347**, 975–982 (2002).
2. Dabbouseh, N. M. & Jensen, D. M. Future therapies for chronic hepatitis C. *Nat Rev Gastroenterol Hepatol* **10**, 268–276 (2013).
3. Muto, Y. *et al.* Prevention of second primary tumors by an acyclic retinoid, polyprenoic acid, in patients with hepatocellular carcinoma. Hepatoma Prevention Study Group. *N Engl J Med* **334**, 1561–1567 (1996).
4. Muto, Y., Moriwaki, H. & Saito, A. Prevention of second primary tumors by an acyclic retinoid in patients with hepatocellular carcinoma. *N Engl J Med* **340**, 1046–1047 (1999).
5. Okada, H. *et al.* Acyclic retinoid targets platelet-derived growth factor signaling in the prevention of hepatic fibrosis and hepatocellular carcinoma development. *Cancer Res* **72**, 4459–4471 (2012).
6. Shimizu, M. *et al.* Acyclic retinoid inhibits diethylnitrosamine-induced liver tumorigenesis in obese and diabetic C57BLKS/J- +(db)/+Lepr(db) mice. *Cancer Prev Res* **4**, 128–136 (2011).
7. Morbitzer, M. & Herget, T. Expression of gastrointestinal glutathione peroxidase is inversely correlated to the presence of hepatitis C virus subgenomic RNA in human liver cells. *J Biol Chem* **280**, 8831–8841 (2005).
8. Yano, M. *et al.* Comprehensive analysis of the effects of ordinary nutrients on hepatitis C virus RNA replication in cell culture. *Antimicrob Agents Chemother* **51**, 2016–2027 (2007).
9. Shimakami, T. *et al.* Stabilization of hepatitis C virus RNA by an Ago2-miR-122 complex. *Proc Natl Acad Sci U S A* **109**, 941–946 (2012).
10. Shimakami, T. *et al.* Protease inhibitor-resistant hepatitis C virus mutants with reduced fitness from impaired production of infectious virus. *Gastroenterology* **140**, 667–675 (2011).

11. Yi, M., Ma, Y., Yates, J. & Lemon, S. M. Compensatory mutations in E1, p7, NS2, and NS3 enhance yields of cell culture-infectious intergenotypic chimeric hepatitis C virus. *J Virol* **81**, 629–638 (2007).
12. Beard, M. R. *et al.* An infectious molecular clone of a Japanese genotype 1b hepatitis C virus. *Hepatology* **30**, 316–324 (1999).
13. Wakita, T. *et al.* Production of infectious hepatitis C virus in tissue culture from a cloned viral genome. *Nat Med* **11**, 791–796 (2005).
14. Alvisi, G., Madan, V. & Bartenschlager, R. Hepatitis C virus and host cell lipids: an intimate connection. *RNA Biol* **8**, 258–269 (2011).
15. Bassendine, M. F., Sheridan, D. A., Bridge, S. H., Felmlee, D. J. & Neely, R. D. Lipids and HCV. *Semin Immunopathol* **35**, 87–100 (2013).
16. Herker, E. & Ott, M. Emerging role of lipid droplets in host/pathogen interactions. *J Biol Chem* **287**, 2280–2287 (2012).
17. Phan, T., Beran, R. K., Peters, C., Lorenz, I. C. & Lindenbach, B. D. Hepatitis C virus NS2 protein contributes to virus particle assembly via opposing epistatic interactions with the E1–E2 glycoprotein and NS3-NS4A enzyme complexes. *J Virol* **83**, 8379–8395 (2009).
18. Bocher, W. O., Wallasch, C., Hohler, T. & Galle, P. R. All-trans retinoic acid for treatment of chronic hepatitis C. *Liver Int* **28**, 347–354 (2008).
19. Bitetto, D. *et al.* Vitamin A deficiency is associated with hepatitis C virus chronic infection and with unresponsiveness to interferon-based antiviral therapy. *Hepatology* **57**, 925–933 (2013).
20. Hamamoto, S. *et al.* 9-cis retinoic acid enhances the antiviral effect of interferon on hepatitis C virus replication through increased expression of type I interferon receptor. *J Lab Clin Med* **141**, 58–66 (2003).
21. Masaki, T. *et al.* Interaction of hepatitis C virus nonstructural protein 5A with core protein is critical for the production of infectious virus particles. *J Virol* **82**, 7964–7976 (2008).
22. Miyanari, Y. *et al.* The lipid droplet is an important organelle for hepatitis C virus production. *Nat Cell Biol* **9**, 1089–1097 (2007).
23. Shimizu, Y. *et al.* Lipoprotein component associated with hepatitis C virus is essential for virus infectivity. *Curr Opin Virol* **1**, 19–26 (2011).
24. Coller, K. E. *et al.* Molecular determinants and dynamics of hepatitis C virus secretion. *PLoS Pathog* **8**, e1002466 (2012).
25. Hishiki, T. *et al.* Infectivity of hepatitis C virus is influenced by association with apolipoprotein E isoforms. *J Virol* **84**, 12048–12057 (2010).
26. Syed, G. H. & Siddiqui, A. Effects of hypolipidemic agent nordihydroguaiaretic acid on lipid droplets and hepatitis C virus. *Hepatology* **54**, 1936–1946 (2011).
27. Ploen, D. *et al.* TIP47 plays a crucial role in the life cycle of hepatitis C virus. *J Hepatol*, (2013).
28. Vogt, D. A. *et al.* Lipid Droplet-Binding Protein TIP47 Regulates Hepatitis C Virus RNA Replication through Interaction with the Viral NS5A Protein. *PLoS Pathog* **9**, e1003302 (2013).
29. Huang, J. T. *et al.* Hepatitis C Virus Replication Is Modulated by the Interaction of Nonstructural Protein NS5B and Fatty Acid Synthase. *J Virol* **87**, 4994–5004 (2013).
30. Fujino, T. *et al.* Expression profile of lipid metabolism-associated genes in hepatitis C virus-infected human liver. *Hepatol Res* **40**, 923–929 (2010).
31. Yang, W. *et al.* Fatty acid synthase is up-regulated during hepatitis C virus infection and regulates hepatitis C virus entry and production. *Hepatology* **48**, 1396–1403 (2008).
32. Lerat, H. *et al.* Hepatitis C virus proteins induce lipogenesis and defective triglyceride secretion in transgenic mice. *J Biol Chem* **284**, 33466–33474 (2009).
33. Waris, G., Felmlee, D. J., Negro, F. & Siddiqui, A. Hepatitis C virus induces proteolytic cleavage of sterol regulatory element binding proteins and stimulates their phosphorylation via oxidative stress. *J Virol* **81**, 8122–8130 (2007).
34. Muto, Y. & Moriwaki, H. Antitumor activity of vitamin A and its derivatives. *J Natl Cancer Inst* **73**, 1389–1393 (1984).
35. Suzui, M. *et al.* Growth inhibition of human hepatoma cells by acyclic retinoid is associated with induction of p21(CIP1) and inhibition of expression of cyclin D1. *Cancer Res* **62**, 3997–4006 (2002).
36. Nakamura, N. *et al.* Induction of apoptosis by acyclic retinoid in the human hepatoma-derived cell line, HuH-7. *Biochem Biophs Res Commun* **207**, 382–388 (1995).
37. Honda, M. *et al.* Peretinoin, an acyclic retinoid, improves the hepatic gene signature of chronic hepatitis C following curative therapy of hepatocellular carcinoma. *BMC cancer* **13**, 191 (2013).
38. Abu-Mouch, S., Fireman, Z., Jarchovsky, J., Zeina, A. R. & Assy, N. Vitamin D supplementation improves sustained virologic response in chronic hepatitis C (genotype 1)-naive patients. *World J Gastroenterol* **17**, 5184–5190 (2011).
39. Bitetto, D. *et al.* Vitamin D supplementation improves response to antiviral treatment for recurrent hepatitis C. *Transpl Int* **24**, 43–50 (2011).
40. Tokiwa, T. *et al.* Differentiation potential of an immortalized non-tumorigenic human liver epithelial cell line as liver progenitor cells. *Cell Biol Int* **30**, 992–998 (2006).
41. Shirasaki, T. *et al.* La protein required for internal ribosome entry site-directed translation is a potential therapeutic target for hepatitis C virus replication. *J Infect Dis* **202**, 75–85 (2010).
42. Shirasaki, T. *et al.* MicroRNA-27a Regulates Lipid Metabolism and Inhibits Hepatitis C Virus Replication in Human Hepatoma Cells. *J Virol* **87**, 5270–5286 (2013).
43. Honda, M., Shimazaki, T. & Kaneko, S. La protein is a potent regulator of replication of hepatitis C virus in patients with chronic hepatitis C through internal ribosomal entry site-directed translation. *Gastroenterology* **128**, 449–462 (2005).

Acknowledgments

We would like to thank Dr T. Wakita (National Institute of Infectious Disease, Tokyo, Japan) for providing the plasmid encoding JFH1, Dr C. Lee (ThinkSCIENCE INC., Tokyo, Japan) for assistance for medical writing and proof-reading, and Ms Y. Terao (Kanazawa University Hospital, Kanazawa, Japan) for making illustrations. This work was partially supported by the Takeda Science Foundation.

Author contributions

Study design and concept; T.S., T.S. and D.Y., Acquisition of data; T.S., T.S., F.L., K.M., T.S., R.T. and M.F., Drafting of the manuscript; T.S. and T.S., Critical revision of the manuscript for important intellectual content; M.H., D.Y., S.M., S.L. and S.K., Study supervision; M.H. and S.K. All authors reviewed the manuscript.

Additional information

Supplementary information accompanies this paper at http://www.nature.com/scientificreports

Competing financial interests: The authors declare no competing financial interests.

How to cite this article: Shimakami, T. *et al.* The Acyclic Retinoid Peretinoin Inhibits Hepatitis C Virus Replication and Infectious Virus Release *in Vitro*. *Sci. Rep.* **4**, 4688; DOI:10.1038/srep04688 (2014).

Cancer Immunol Immunother (2014) 63:347–356
DOI 10.1007/s00262-013-1514-7

ORIGINAL ARTICLE

In vivo immunological antitumor effect of OK-432-stimulated dendritic cell transfer after radiofrequency ablation

Hidetoshi Nakagawa · Eishiro Mizukoshi · Noriho Iida · Takeshi Terashima · Masaaki Kitahara · Yohei Marukawa · Kazuya Kitamura · Yasunari Nakamoto · Kazumasa Hiroishi · Michio Imawari · Shuichi Kaneko

Received: 1 June 2013 / Accepted: 17 December 2013 / Published online: 3 January 2014

Abstract Radiofrequency ablation therapy (RFA) is a radical treatment for liver cancers and induces tumor antigen-specific immune responses. In the present study, we examined the antitumor effects of focal OK-432-stimulated dendritic cell (DC) transfer combined with RFA and analyzed the functional mechanisms involved using a murine model. C57BL/6 mice were injected subcutaneously with colon cancer cells (MC38) in their bilateral flanks. After the establishment of tumors, the subcutaneous tumor on one flank was treated using RFA, and then OK-432-stimulated DCs were injected locally. The antitumor effect of the treatment was evaluated by measuring the size of the tumor on the opposite flank, and the immunological responses were assessed using tumor-infiltrating lymphocytes, splenocytes and draining lymph nodes. Tumor growth was strongly inhibited in mice that exhibited efficient DC migration after RFA and OK-432-stimulated DC transfer, as compared to mice treated with RFA alone or treatment involving immature DC transfer. We also demonstrated that the antitumor effect of this treatment depended on both CD8-positive and CD4-positive cells. On the basis of our findings, we believe that combination therapy for metastatic liver cancer consisting of OK-432-stimulated DCs in combination with RFA can proceed to clinical trials, and it is anticipated to be markedly superior to RFA single therapy.

Keywords Metastatic liver cancer · MC38 · Immunotherapy · Intratumoral injection · Tumor-infiltrating lymphocyte

Abbreviations

RFA	Radiofrequency ablation
DC	Dendritic cell
HCC	Hepatocellular carcinoma
TAE	Transcatheter hepatic arterial embolization
TLR	Toll-like receptor
GFP	Green fluorescent protein
ELISPOT	Enzyme-linked immunospot
Treg	Regulatory T cell
MDSC	Myeloid-derived suppressor cell
IFN-γ	Interferon-γ

Introduction

Liver is one of the most common organs to which various cancers spread from their site of origin. In some types of cancer, the liver metastasis lesion is a target of surgical treatment. For instance, surgical resection of hepatic metastasis achieves longer median survival in colorectal and breast cancer patients [1, 2]. However, even if the hepatic lesions are surgically treated, the prognosis of the

Electronic supplementary material The online version of this article (doi:10.1007/s00262-013-1514-7) contains supplementary material, which is available to authorized users.

H. Nakagawa · E. Mizukoshi · N. Iida · T. Terashima · M. Kitahara · Y. Marukawa · K. Kitamura · S. Kaneko (✉)
Disease Control and Homeostasis, Graduate School of Medical Sciences, Kanazawa University, 13-1 Takara-machi, Kanazawa, Ishikawa 920-8641, Japan
e-mail: skaneko@m-kanazawa.jp

H. Nakagawa
e-mail: hidetoshi.naka@gmail.com

Y. Nakamoto
Second Department of Internal Medicine, Faculty of Medical Sciences, University of Fukui, Fukui 910-1193, Japan

K. Hiroishi · M. Imawari
Shin-yurigaoka General Hospital, Kawasaki, Kanagawa 215-0026, Japan

patients is not satisfactory. As for colorectal cancers, the recurrence rate is over 50 % after radical resection of metastatic lesions [3]. Moreover, at the time of initial diagnosis, only a few patients meet the criteria for hepatic resection because of unresectability, low hepatic functional reserve or poor performance status [4].

Radiofrequency ablation therapy (RFA) has been developed as a radical and minimally invasive treatment method for metastatic liver cancers. Recently, RFA has been used as an adjunct to hepatic resection or as an alternative method to resection when surgical treatment is not feasible [5]. Additionally, it has been revealed that RFA for metastatic liver cancers generates tumor antigen-specific T-cell responses in man [6, 7]. We have previously reported that RFA could also control distant tumor growth in a murine hepatocellular carcinoma (HCC) model [8].

Dendritic cells (DCs) are potent antigen-presenting cells [9]. Recently, we have established new treatments using local DC injection with transcatheter hepatic arterial embolization (TAE) and have shown that this combination therapy could induce tumor antigen-specific T-cell responses in HCC patients [10].

OK-432 is derived from the Su strain of Group A *Streptococcus pyogenes* by means of treatment with benzylpenicillin and heat [11]. OK-432 can stimulate DCs via Toll-like receptor (TLR) 3, TLR4 and β2 integrin and subsequently induce antigen-specific cytotoxic lymphocytes [12–14].

On the basis of these results, we hypothesized that OK-432-stimulated DC transfer is a promising candidate for an enhancer that can strongly increase the antitumor effect of RFA. We have previously demonstrated in a clinical trial that the local infusion of OK-432-stimulated DC after TAE could prolong recurrence-free survival in HCC patients [15]. However, it remains unknown as to how the transferred DCs work in combination with RFA. In the present study, we examined the antitumor effects of OK-432-stimulated DCs when combined with RFA and analyzed the functional mechanisms involved using a murine subcutaneous colon cancer model.

Materials and methods

Animals

Wild-type 8–12-week-old female C57BL/6 J mice were obtained from Charles River Japan (Yokohama, Japan). Female C57BL/6-Tg (UBC-GFP) 30Scha/J mice were purchased from the Jackson Laboratory (Bar Harbor, ME, USA). All animal experiments were approved and performed in accordance with the Guidelines for the Care and Use of Laboratory Animals of Kanazawa University, which strictly conforms to the Guide for the Care and Use of Laboratory Animals published by the US National Institutes of Health.

Cell lines and bone marrow-derived dendritic cells

A murine colorectal cancer cell line, MC38 and hybridomas, clone GK1.5 and clone 2.43 were cultured in RPMI-1640 containing 10 % fetal bovine serum (Life Technologies, Co., Carlsbad, CA, USA) supplemented with 100 μg/ml streptomycin and 100 units/ml penicillin (Wako Pure Chemical Industries Ltd., Osaka, Japan). Bone marrow-derived dendritic cells (BMDCs) were generated using 20 ng/ml of recombinant granulocyte macrophage colony-stimulating factor (R&D Systems, Minneapolis, MN, USA) as previously described [16]. OK-432 (Picibanil; Chugai Pharmaceutical Co. Ltd., Tokyo, Japan) was loaded into the supernatant from days 6–7 of the BMDC generation period at a concentration of 5 μg/ml.

In vitro evaluation of phagocytic activity by dendritic cells

MC38 cells were labeled with DiD dye (Life Technologies) according to the manufacturer's instructions followed by heat treatment at 80 °C for 90 s. OK-432-stimulated or immature DCs were co-incubated with the treated MC38 cells for 3 h at a ratio of 1:1. After incubation, the cell suspensions were observed using a fluorescence microscope (BZ9000: Keyence, Osaka, Japan) and analyzed by means of FACSCalibur (BD Immuno-Cytometry System, San Jose, CA, USA).

Animal model

Bilateral flanks of C57BL/6 mice were each injected subcutaneously with 1×10^6 MC38 cells. Seven days after injection, after they had grown to 5–6 mm in diameter, the subcutaneous tumors on one flank were treated using RFA, and 1×10^7 immature DCs or 1×10^7 OK-432-stimulated DCs were injected into the treated tumors at 24 h after RFA. After this, the volume of the untreated tumor on the contralateral flank was evaluated over a period of 10 days. Tumor volumes were calculated using the following formula: tumor volume (mm^3) = (longest diameter) × (shortest diameter)^2/2.

Radiofrequency ablation

Mice bearing tumors were anesthetized with an intraperitoneal injection of pentobarbital (Kyoritsu Seiyaku, Tokyo, Japan), and the skin on the tumor was cut. Subsequently, an expandable RFA needle was inserted into the tumor, which was treated using a radiofrequency generator (RITA

500PA; RITA Medical Systems, Inc., Fremont, CA, USA). During the use of this system, the intratumor temperature was maintained at 70–90 °C, and the current was turned off when the tumor exhibited heat denaturation.

Flow cytometry

The DCs were detected by means of staining with anti-CD11c antibodies (Life technologies). The lymphocytes in the draining lymph node were stained with anti-CD4 antibodies, anti-CD8 antibodies, anti-CD11c antibodies and anti-CD69 antibodies (BD Bioscience, San Diego, CA, USA). The splenocytes were stained with anti-CD4 antibodies, anti-CD8 antibodies, CD11c antibodies, anti-NK1.1 antibodies, CD45 antibodies (BD Bioscience), anti-Gr-1 antibodies, and anti-CD11b antibodies and mouse regulatory T-cell staining solution (BioLegend, San Diego, CA, USA). The stained samples were analyzed using FACSAria II (BD Immuno-Cytometry System).

Immunohistochemical assay

The draining lymph nodes and the observed tumors were embedded in Sakura Tissue-Tek optimum cutting temperature compound (Sakura Finetek Japan Co., Ltd., Tokyo, Japan) for frozen sectioning. Tissue sections were fixed at −20 °C in methanol for 10 min. The draining lymph nodes were stained using rabbit anti-GFP antibody (Abcam, Cambridge, UK) that were detected using an EnVision+/HRP kit (Dako, Glostrup, Denmark). The observed tumors were stained with anti-CD4 and anti-CD8a (BD Bioscience), which were detected using the Nichirei Histofine Simple Stain Mouse Max PO (Rat) system (Nichirei Co., Tokyo, Japan) or the Vectastain ABC kit (Vector Laboratory, Inc., Burlingame, CA, USA).

Interferon gamma enzyme-linked immunospot assay

The splenocytes, the tumor-infiltrating lymphocytes (TILs) in the untreated tumors that were isolated by mechanical homogenizations and density gradient centrifugations, and the lymphocytes in the draining lymph nodes were loaded into the interferon gamma enzyme-linked immunospot assay to estimate the tumor-specific immune reactions, as previously described [8, 17]. Briefly, 3×10^5 lymphocytes or 1×10^5 TILs were incubated for 24 h with or without 6×10^5 MC38 lysates, which were prepared through five cycles of rapid freezing in liquid nitrogen, thawing at 55 °C and centrifugation. The number of MC38-specific IFN-γ spots was determined by subtracting the number of spots incubated without MC38 lysates from the number of spots incubated with MC38 lysates. For CD4 or CD8 depletion, we used magnetic CD4 beads or CD8 beads (Miltenyi Biotec, Bergisch Gladbach, Germany).

In vivo CD4/CD8 depletion

For in vivo CD4 or CD8 depletion, B6 mice were injected intraperitoneally with 200 μg of purified monoclonal antibodies specific to CD4 or CD8 at 1 day before and 3 days after RFA treatment; the monoclonal antibodies were prepared from GK1.5 hybridoma and 2.43 hybridoma, respectively [18]. The depletion was confirmed by flow cytometry using peripheral blood lymphocytes stained with anti-CD4 and anti-CD8 antibodies.

Statistical analysis

The data obtained were analyzed statistically using the t test or one-way analysis of variance followed by Tukey's multiple-comparison test. A P value <0.05 was considered as being statistically significant.

Results

Migration efficacy and phagocytic ability of OK-432-stimulated DCs

We employed OK-432 as a modifying agent for DCs, because we have previously shown in clinical studies that OK-432 prolonged recurrence-free survival after combination therapy involving DC injection with TAE for HCC patients [10, 15]. We first confirmed that the OK-432-stimulated murine DCs showed higher expression of maturation markers such as CD40, CD80, CD86, MHC class II and CCR7 (Supplementary Fig. 1), as previously reported [19, 20].

To evaluate their phagocytic abilities, we incubated the immature DCs and the OK-432-stimulated DCs with MC38 tumor cells. Heat-treated MC38 cells were taken up well by both immature DCs and OK-432-stimulated DCs, as compared to nontreated MC38 cells (Fig. 1a–c). In addition, the phagocytic ability of OK-432-stimulated DCs was not inferior to that of immature DCs. These results were consistent with the dextran uptake assay (Supplementary Fig. 2) and our previous data on human monocyte-derived DCs [15]. Since heat-treated MC38 cells were thought to be in a similar condition to those in the MC38 tumor in mice treated with RFA, OK-432-stimulated DCs were expected to effectively phagocytose RFA-treated MC38 tumor cells in vivo.

We next estimated the kinetics of the transferred DCs in mice bearing subcutaneous MC38 tumors treated with RFA. Immature DCs or OK-432-stimulated DCs that were derived from GFP-Tg mice were injected intratumorally

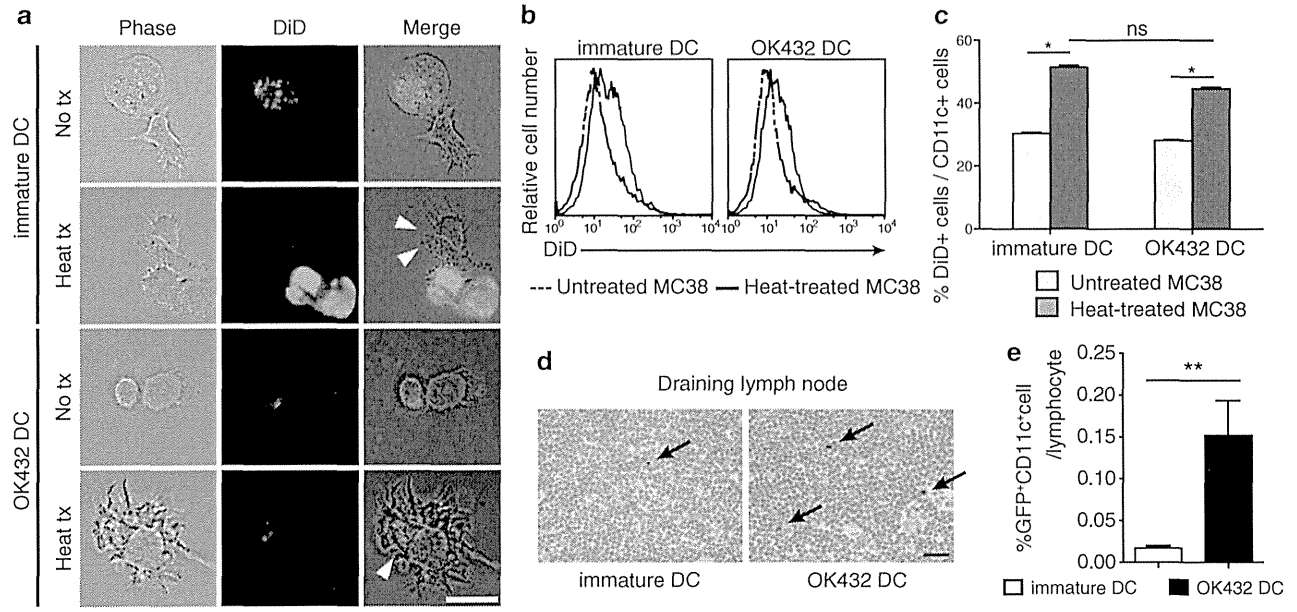

Fig. 1 Effects of OK-432 on murine bone marrow-derived DCs. **a** OK-432-stimulated DCs or immature DCs were co-incubated for 3 h with MC38 cells untreated or treated at 80 °C for 90 s after staining with DiD dye. After incubation, DC and MC38 cells were observed using a fluorescence microscope. *Arrowheads* indicate MC38 derivatives being phagocytosed by DCs. No tx, untreated MC38 cells; heat tx, heat-treated MC38 cells; *bar*, 20 μm. **b**, **c** Co-incubated MC38 cells and DCs were stained with anti-CD11c antibodies and analyzed using flow cytometry. The *histograms* show the DiD fluorescent intensity of the CD11c-positive fractions. The percentages of DiD^+ $CD11c^+$ cells in the $CD11c^+$ cell population are also shown in a *column graph*. The experiments were performed five times, and representative results are shown. Data are presented as the mean ± SE. $^*P < 0.05$. **d** The migration abilities of the DCs after intratumoral transfer were evaluated. The draining lymph nodes were harvested at 3 days after RFA followed by the DC transfer. Frozen sections were prepared and stained with anti-GFP antibodies. *Arrows* indicate the GFP-positive cells in the lymph nodes. *Bar* 20 μm. **e** The draining lymph nodes were also analyzed using flow cytometry after staining with anti-CD11c antibodies. Data were obtained from six mice in each group. Percentages of GFP^+ $CD11c^+$ cell are presented as the mean ± SE. $^{**}P < 0.01$

at 24 h after RFA treatment, and the subcutaneous tumors and the lymph nodes were harvested at 3 days after RFA. According to the immunohistochemical study involving the detection of GFP, the inguinal lymph node on the RFA-treated flank was thought to be the draining lymph node (Supplementary Fig. 3). Additionally, the number of transferred DCs in the draining lymph nodes was significantly higher in the mice treated with the OK-432-stimulated DCs than in those treated with the immature DCs (Fig. 1d, e). Our experimental results attested to the fact that the OK-432-stimulated DCs had both sufficient phagocytic ability and higher migration efficacy.

Effect of RFA in combination with the injection of OK-432-stimulated DCs on tumor growth

OK-432-stimulated DCs were used in combination therapy with RFA in this murine model (Fig. 2a). Namely, BMDCs stimulated with OK-432 were injected into RFA-treated tumor at 24 h after RFA treatment. We compared four groups of tumor-bearing mice as follows: (1) no treatment; (2) RFA only; (3) RFA with the injection of immature DCs; and (4) RFA with the injection of OK-432-stimulated DCs. Tumor volumes were measured for 10 days after treatment/no treatment. On the day after RFA, the treated tumors were covered with scars, started to shrink and had disappeared macroscopically at 4 days after RFA in all of the groups. This indicated that RFA treatment was highly effective for focal lesions. The injected DCs were detected in the treated tumors (Supplementary Fig. 3). With regard to the untreated tumors, as we previously reported, the group treated with RFA only showed an antitumor effect against distant tumors. The injection of immature DCs combined with RFA did not show any additional enhancement of the antitumor effect. On the other hand, the volumes of the untreated tumors in the group that underwent RFA combined with the injection of OK-432-stimulated DCs were strongly suppressed ($P < 0.001$) relative to other groups (Fig. 2b).

Recruitment of antigen-specific lymphocyte fractions in both splenocytes and tumor by injected OK-432-stimulated DCs

Ten days after RFA, the tumors and the spleens were harvested and analyzed using immunohistochemical staining.

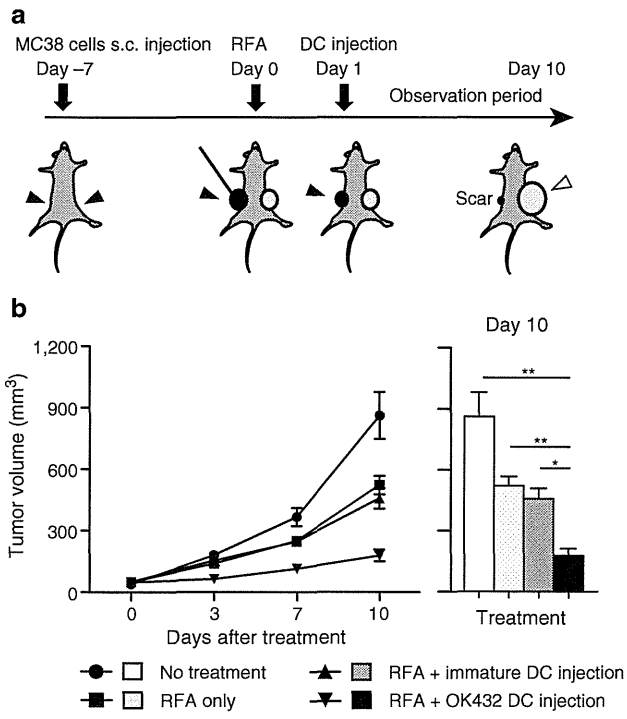

Fig. 2 Impact of injection of OK-432-stimulated DCs into murine MC38 subcutaneous tumors. **a** RFA was administered to a tumor on one flank followed by injection of 1×10^7 DCs into the treated tumor. The untreated tumor on the opposite flank was observed for 10 days. The *solid arrowheads* indicate the treatment intervention sites, and the *open arrowhead* indicates the observed untreated tumor. **b** The tumor volumes were compared among the four groups as follows: (1) no treatment; (2) RFA only; (3) RFA in combination with immature DC injection; and (4) RFA in combination with OK-432-stimulated DC injection. $n = 8$ mice per group. The data are presented as the mean ± SE. $^*P < 0.05$; $^{**}P < 0.001$

We examined the number of tumor-infiltrating CD4-positive or CD8-positive cells in the tumors by means of immunohistochemistry. The infiltration of these cells into the untreated tumors was found to be promoted by RFA. The injection of OK-432-stimulated DCs after RFA induced the additional recruitment of CD8-positive cells into the untreated tumors (Fig. 3a, b). CD11c-, CD11b- and NK1.1-positive cells were very marginal and showed no differences in number among the four groups (data not shown).

Systemically, in terms of analyzing splenocytes with flow cytometry, the number of CD4-positive and CD8-positive cells increased in the group treated with RFA in combination with OK-432-stimulated DCs. On the other hand, the CD11c and NK1.1 fractions, which were considered as DCs and NK cells, respectively, presented no difference among the four groups (Fig. 3c). In addition, we examined the effect of the injection of OK-432-stimulated DCs after RFA on inhibitory blood cells such as regulatory T cells (Tregs) and myeloid-derived suppressor cells (MDSCs) (Fig. 3c). Among CD4-positive cells, significantly fewer Tregs were detected in the group treated with RFA in combination with OK-432-stimulated DCs than in the group treated with RFA in combination with immature DCs. In the analysis of MDSCs, their rates of occurrence were not affected by treatment with either RFA alone or RFA in combination with DCs. Taking these results together, we concluded that treatment with RFA combined with OK-432-stimulated DCs enhanced the number of CD4- or CD8-positive T cells and reduced the Treg/CD4 ratio, but did not influence MDSC numbers.

Furthermore, we examined the number of tumor-specific IFN-γ-producing cells at 10 days after RFA using the ELISPOT assay. The number of IFN-γ-producing cells among splenocytes and TILs showed the same trend as the level of tumor growth control among the four groups (Fig. 3d); the group treated with RFA in combination with injected OK-432 DCs showed the most abundant specific spots. These results suggested that the augmented antitumor effects of RFA combined with OK-432-stimulated DCs depended in large part on tumor-specific immune responses by CD4 cells or CD8 cells.

Evaluation of tumor-specific immune responses in the draining lymph node after OK-432-stimulated DC transfer

CD4 T cells and CD8 T cells are now thought to have an important antitumor effect as a result of the OK-432-stimulated DC transfer. To elucidate the priming of the antigen-specific immune response, we analyzed the draining lymph nodes at 3 days after RFA focusing on CD4-positive or CD8-positive cells. CD69, the early activation marker, on CD4-positive and CD8-positive cells was examined and compared between the immature DC transfer group and the OK-432-stimulated DC transfer group. It was found that CD69 expression on both CD4-positive and CD8-positive cells was elevated in the OK-432-stimulated DC transfer group (Fig. 4a, b). The activations were also demonstrated to be tumor-specific using the IFN-γ ELISPOT assay in which each of CD4-negative and CD8-negative fractions was applied to the assay and both showed tumor-specific IFN-γ secretions (Fig. 4c).

Evaluation of the relationship between CD4-positive and CD8-positive cells and the antitumor effects of RFA and OK-432-stimulated DC transfer

We have demonstrated that combination therapy involving RFA and OK-432-stimulated DC transfer might generate enhanced antitumor effects via tumor-specific CD4-positive and CD8-positive cells. To obtain further evidence, we carried out in vivo CD4 or CD8 depletion studies in mice. Initially, we confirmed CD4 or CD8 depletion in the control in vivo study (Supplementary Fig. 4). The

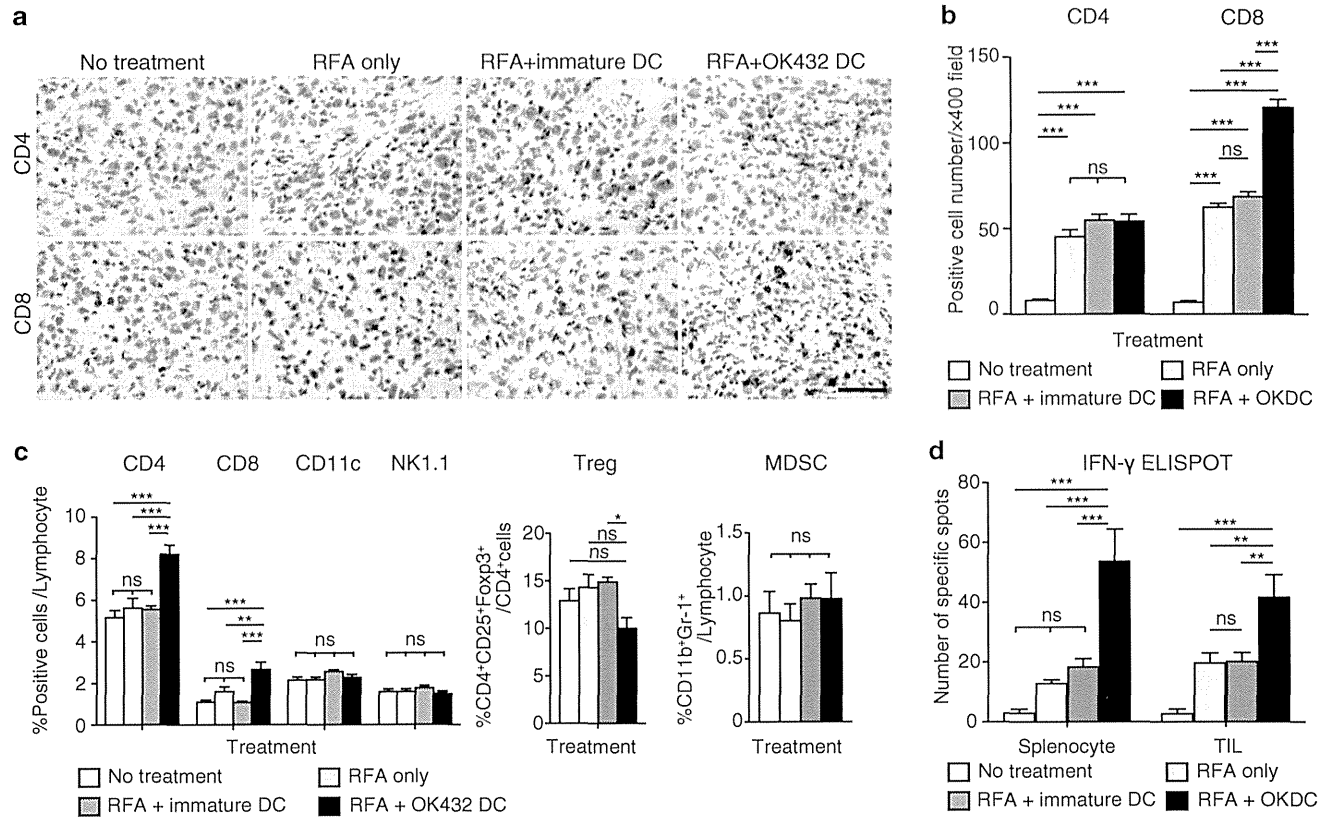

Fig. 3 Analysis of the tumor-infiltrating lymphocytes and the splenocytes after combination therapy with RFA and DC injection. **a** CD4-positive and CD8-positive cells in the observed untreated tumors were detected using immunohistochemistry at 10 days after RFA. The *black bar* represents 50 μm. **b** The number of positive cells was counted using a microscope. This was achieved by counting the number of cells in six randomly chosen tumor areas at 400-fold magnification. Three mice were used in each group. The data are presented as the mean ± SE. *** $P < 0.001$; *ns* not significant. **c** Ten days after RFA, splenocytes were stained with anti-CD4, anti-CD8, anti-NK1.1 and anti-CD11c antibodies and analyzed using flow cytometry. Regulatory T cells (Tregs) defined as $CD4^+CD25^+Foxp3^+$ cells and myeloid-derived suppressor cells (MDSCs) defined as $CD11b^+Gr\text{-}1^+$ cells were counted and compared among the four groups. Six mice were analyzed in each group. The data are presented as the mean ± SE. *$P < 0.05$; **$P < 0.01$; ***$P < 0.001$; *ns* not significant. **d** Immune responses by the splenocytes and the tumor-infiltrating lymphocytes (TILs) were examined by means of the IFN-γ enzyme-linked immunospot (ELISPOT) assay using MC38 lysate. In the assay for TILs, 1×10^5 TILs were mixed with 2×10^5 splenocytes from B6 mice and applied to the well. Six mice were analyzed in each group. The data are presented as the mean ± SE. **$P < 0.01$; ***$P < 0.001$; *ns* not significant

CD4-positive and CD8-positive fractions in the peripheral blood were greatly depleted at 7 days after injection of the antibodies. The experimental schedule was determined as follows. The depletion antibodies were injected at 1 day before and 3 days after RFA, and the tumors that were not treated with RFA were observed for 10 days. In addition, the draining lymph nodes were harvested at 3 days after RFA and analyzed (Supplementary Fig. 5). The antitumor effects of RFA treatment and the augmented effects from OK-432-stimulated DCs were cancelled out by depletion of both CD4 and CD8 cells (Fig. 5a). In the CD4 depletion study, there was no priming of the antitumor effect in the draining lymph nodes (Fig. 5b; Supplementary Fig. 6). On the other hand, in the CD8 depletion study CD4 cells were activated with tumor specificities in the draining lymph node in both groups, and the activation was stronger in the OK-432-stimulated DC transfer group (Fig. 5b; Supplementary Fig. 6). Tumor-specific reactions were also demonstrated in the splenocytes and the TILs at 10 days after RFA. There was a tendency for OK-432 DC transfer treatment to result in the recruitment of increased numbers of tumor-specific lymphocytes into the tumor on the opposite flank ($P = 0.184$; Fig. 5c). These results indicated that the tumor-specific activation of CD8 cells was necessary for the antitumor effect and was completely dependent on help from the CD4 cells.

Discussion

In the past decade, cytotoxic agents and molecular-targeted therapies have been developed, and the treatment outcomes

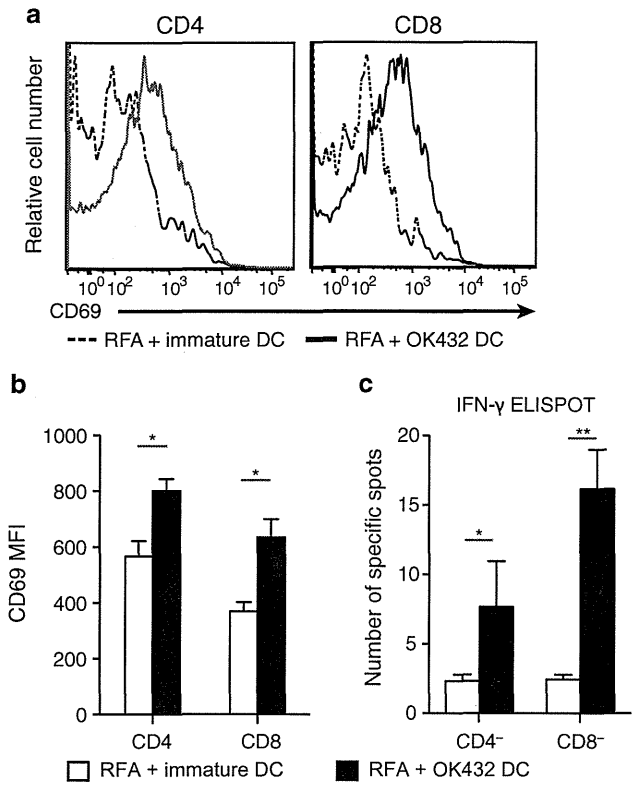

Fig. 4 Antigen-specific activation of both CD4-positive and CD8-positive cells in the draining lymph node. **a** Three days after RFA followed by DC transfer, the draining lymph node was harvested and analyzed by staining with anti-CD4 antibodies, anti-CD8 antibodies and anti-CD69 antibodies. The fluorescence intensities of CD69 in the CD4-positive and CD8-positive fractions are compared between the OK-432-stimulated DC transfer group and the immature DC transfer group. The data were obtained from six mice in each group. The *histograms* show the representative data. **b** The mean fluorescent intensities are also presented as the mean ± SE. $*P < 0.05$. **c** The antigen specificities of the T-cell activations were confirmed by means of the IFN-γ ELISPOT assay using MC38 lysate. After CD4 or CD8 depletion using CD4 and CD8 magnetic beads, the lymphocytes from the draining lymph nodes were submitted to IFN-γ ELISPOT assay. Data were obtained from six mice in each group. $*P < 0.05$; $**P < 0.01$

for various cancers have improved. However, few patients with advanced cancers have been completely cured, and thus, new strategies for anticancer therapy are required. Immunotherapy is considered to have the potential to effectively treat such advanced cancers, and many different approaches have been explored. For the utilization of the adoptive immune response in a cancer therapy, DCs are a key constituent of the immune system. This is because of their natural potential to present tumor-associated antigens to $CD4^+$ and $CD8^+$ lymphocytes and also to control both immune tolerance and immunity [21]. Thus, DCs are considered as an important target for cancer immunotherapy. Many trials and studies have been carried out regarding immunotherapy for cancer using DCs, some of which have been reported to have pronounced effects [22–25]. In recent studies, it has been revealed that RFA treatment induces tumor-specific T-cell responses, which is known as the abscopal effect; this has been mainly reported in radiotherapy studies and is augmented with combined immunotherapies [26, 27]. Brok et al. [28] have previously reported on the vaccination effects of combination therapy involving RFA and CTLA-4 antibody.

To our knowledge, this is the first study that has demonstrated using a murine metastatic cancer model that RFA in combination with focal DC injection could enhance the antitumor effects of RFA alone. Our results showed that immature DCs made no additional immunological contribution to RFA. In the analysis of draining lymph nodes, few transferred DCs were detected after the injection of immature DCs. It appeared that immature DCs did not act as sentinels in the adoptive immune system, partially because they exhibited low expression of CCR7 (the main molecule that promotes DC migration [29]), even though elevation of CCR7 expression using OK-432 was very modest in our study. There is another possibility immature DCs are easily lysed and excluded by the host immune system [30]. On the other hand, mature DCs can escape cell lysis [31].

Utilization of OK-432-stimulated DCs improved the number of migrating transferred DCs in the present study. These DCs, which could act as sentinels for immunity, induced expansion in the number of tumor-specific lymphocytes in the draining lymph nodes, in the splenocytes and in the distant nontreated tumors, without systemic expansion of inhibitory cells such as Tregs or MDSCs. We also demonstrated that these augmented antitumor effects after OK-432-stimulated DC transfer were primed in the draining lymph nodes with tumor-specific activations of CD4-positive and CD8-positive cells; it was proved that without CD4-positive or CD8-positive cells, both the antitumor effect by RFA and the additional effect of the injection of OK-432-stimulated DCs disappeared completely. In addition, the in vivo CD4 depletion study revealed that tumor-specific activations of CD8-positive cells were not seen in the draining lymph nodes in both groups after the injection of immature DCs and OK-432-stimulated DC injection; in other words, tumor-specific CD8 activation depended on CD4-positive cells entirely. In the CD8 depletion study, on the other hand, we found that tumor-specific CD4-positive cells appeared in the draining lymph nodes, the splenocyte population and the untreated tumor on the opposite flank, and these lymphocytes were considered to be CD4-positive cells. In the tumor-infiltrating lymphocytes, there was a tendency for more tumor-specific CD4-positive cells to be recruited after treatment involving OK-432-stimulated DC transfer. Many researchers have demonstrated the contribution of CD4 cells to cytotoxicity

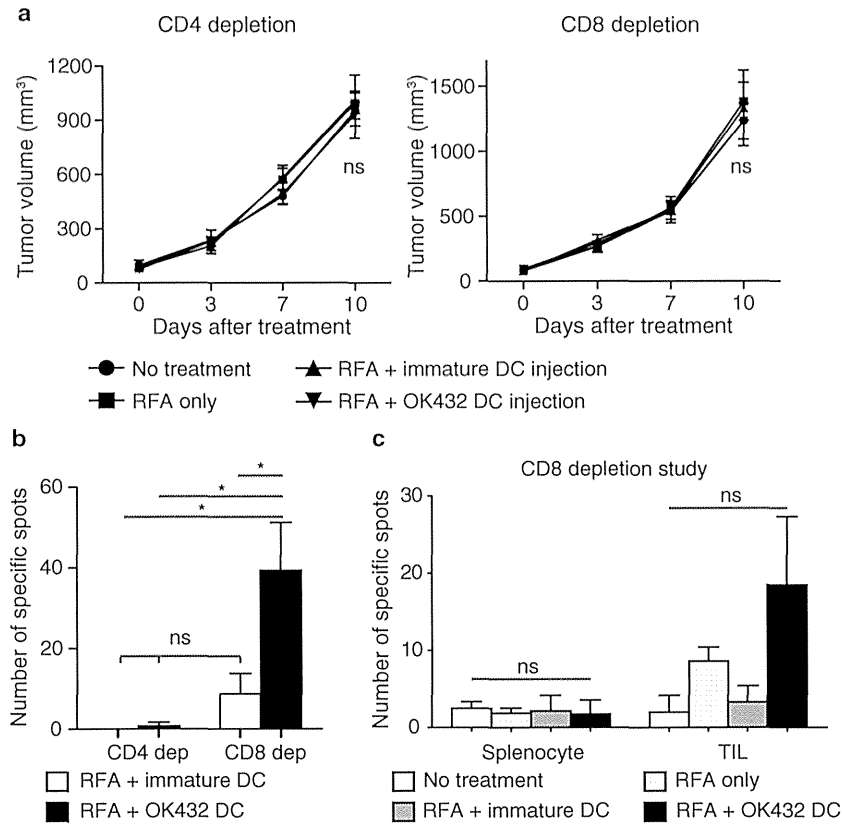

Fig. 5 The augmented antitumor effects depended on both CD4-positive and CD8-positive cells. **a** For in vivo CD4 or CD8 depletion, monoclonal antibodies specific to CD4 (GK1.5) or CD8 (2.43), respectively, were injected intraperitoneally at 1 day before and 3 days after RFA. Tumor volumes were compared among the four groups for 10 days after RFA. In each experiment, data were obtained from four mice per group and are presented as the mean ± SE. *ns* not significant. **b** The draining lymph nodes were harvested at 3 days after RFA and analyzed for their tumor specificities using the IFN-γ ELISPOT assay. Two mice were used in each group. Data are shown as the mean ± SE. $*P < 0.005$; *ns* not significant. **c** In the CD8 depletion study, splenocytes and tumor-infiltrating lymphocytes (TILs) were evaluated for their tumor specificities using the IFN-γ ELISPOT assay as described in Fig. 3. Four mice were used in each group. Data are shown as the mean ± SE. *ns* not significant

[32, 33]. However, in our experimental models, tumor-specific CD4-positive cells were not observed to contribute to the antitumor effect. Summarizing the above, in our study, the CD4-positive cells were required for the priming of the immune responses, and the CD8-positive cells acted as the effector cells after help from the CD4-positive cells.

In conclusion, we consider on the basis of our preclinical findings regarding combination therapy involving OK-432-stimulated DCs with RFA for the treatment of metastatic liver cancer that clinical trials can now proceed. It is anticipated that this combination therapy will be markedly superior to RFA single therapy.

Acknowledgments The authors thank Ms. Fushimi and Ms. Baba for technical support. This study was supported by research grants from the Ministry of Education, Culture, Sports, Science and Technology of Japan.

Conflict of interest The authors received financial support for this study from Chugai Pharmaceutical Co., Ltd.

References

1. Ruiterkamp J, Ernst MF, de Munck L, van der Heiden, van der Loo M, Bastiaannet E, van de Poll-Franse LV, Bosscha K, Tjan-Heijnen VC, Voogd AC (2011) Improved survival of patients with primary distant metastatic breast cancer in the period of 1995–2008. A nationwide population-based study in the Netherlands. Breast Cancer Res Treat 128(2):495–503. doi:10.1007/s10549-011-1349-x
2. Simmonds PC, Primrose JN, Colquitt JL, Garden OJ, Poston GJ, Rees M (2006) Surgical resection of hepatic metastases from colorectal cancer: a systematic review of published studies. Br J Cancer 94(7):982–999. doi:10.1038/sj.bjc.6603033
3. Nordlinger B, Guiguet M, Vaillant JC, Balladur P, Boudjema K, Bachellier P, Jaeck D (1996) Surgical resection of colorectal carcinoma metastases to the liver. A prognostic scoring system to improve case selection, based on 1568 patients. Association Francaise de Chirurgie. Cancer 77(7):1254–1262
4. Bentrem DJ, Dematteo RP, Blumgart LH (2005) Surgical therapy for metastatic disease to the liver. Annu Rev Med 56:139–156. doi:10.1146/annurev.med.56.082103.104630
5. Meyers MO, Sasson AR, Sigurdson ER (2003) Locoregional strategies for colorectal hepatic metastases. Clin Colorectal Cancer 3(1):34–44. doi:10.3816/CCC.2003.n.010

6. Napoletano C, Taurino F, Biffoni M, De Majo A, Coscarella G, Bellati F, Rahimi H, Pauselli S, Pellicciotta I, Burchell JM, Gaspari LA, Ercoli L, Rossi P, Rughetti A (2008) RFA strongly modulates the immune system and anti-tumor immune responses in metastatic liver patients. Int J Oncol 32(2):481–490
7. Nobuoka D, Motomura Y, Shirakawa H, Yoshikawa T, Kuronuma T, Takahashi M, Nakachi K, Ishii H, Furuse J, Gotohda N, Takahashi S, Nakagohri T, Konishi M, Kinoshita T, Komori H, Baba H, Fujiwara T, Nakatsura T (2012) Radiofrequency ablation for hepatocellular carcinoma induces glypican-3 peptide-specific cytotoxic T lymphocytes. Int J Oncol 40(1):63–70. doi:10.3892/ijo.2011.1202
8. Iida N, Nakamoto Y, Baba T, Nakagawa H, Mizukoshi E, Naito M, Mukaida N, Kaneko S (2010) Antitumor effect after radiofrequency ablation of murine hepatoma is augmented by an active variant of CC Chemokine ligand 3/macrophage inflammatory protein-1 alpha. Cancer Res 70(16):6556–6565. doi:10.1158/0008-5472.CAN-10-0096
9. Banchereau J, Briere F, Caux C, Davoust J, Lebecque S, Liu YJ, Pulendran B, Palucka K (2000) Immunobiology of dendritic cells. Annu Rev Immunol 18:767–811. doi:10.1146/annurev.immunol.18.1.767
10. Nakamoto Y, Mizukoshi E, Tsuji H, Sakai Y, Kitahara M, Arai K, Yamashita T, Yokoyama K, Mukaida N, Matsushima K, Matsui O, Kaneko S (2007) Combined therapy of transcatheter hepatic arterial embolization with intratumoral dendritic cell infusion for hepatocellular carcinoma: clinical safety. Clin Exp Immunol 147(2):296–305. doi:10.1111/j.1365-2249.2006.03290.x
11. Ryoma Y, Moriya Y, Okamoto M, Kanaya I, Saito M, Sato M (2004) Biological effect of OK-432 (picibanil) and possible application to dendritic cell therapy. Anticancer Res 24(5C):3295–3301
12. Nakahara S, Tsunoda T, Baba T, Asabe S, Tahara H (2003) Dendritic cells stimulated with a bacterial product, OK-432, efficiently induce cytotoxic T lymphocytes specific to tumor rejection peptide. Cancer Res 63(14):4112–4118
13. Okamoto M, Oshikawa T, Tano T, Ahmed SU, Kan S, Sasai A, Akashi S, Miyake K, Moriya Y, Ryoma Y, Saito M, Sato M (2006) Mechanism of anticancer host response induced by OK-432, a streptococcal preparation, mediated by phagocytosis and Toll-like receptor 4 signaling. J Immuno ther 29(1):78–86
14. Hovden AO, Karlsen M, Jonsson R, Appel S (2012) The bacterial preparation OK432 induces IL-12p70 secretion in human dendritic cells in a TLR3 dependent manner. PLoS ONE 7(2):e31217. doi:10.1371/journal.pone.0031217
15. Nakamoto Y, Mizukoshi E, Kitahara M, Arihara F, Sakai Y, Kakinoki K, Fujita Y, Marukawa Y, Arai K, Yamashita T, Mukaida N, Matsushima K, Matsui O, Kaneko S (2011) Prolonged recurrence-free survival following OK432-stimulated dendritic cell transfer into hepatocellular carcinoma during transarterial embolization. Clin Exp Immunol 163(2):165–177. doi:10.1111/j.1365-2249.2010.04246.x
16. Inaba K, Inaba M, Romani N, Aya H, Deguchi M, Ikehara S, Muramatsu S, Steinman RM (1992) Generation of large numbers of dendritic cells from mouse bone marrow cultures supplemented with granulocyte/macrophage colony-stimulating factor. J Exp Med 176(6):1693–1702
17. Mizukoshi E, Nakamoto Y, Marukawa Y, Arai K, Yamashita T, Tsuji H, Kuzushima K, Takiguchi M, Kaneko S (2006) Cytotoxic T cell responses to human telomerase reverse transcriptase in patients with hepatocellular carcinoma. Hepatology 43(6):1284–1294. doi:10.1002/hep.21203
18. Nakamoto Y, Suda T, Momoi T, Kaneko S (2004) Different procarcinogenic potentials of lymphocyte subsets in a transgenic mouse model of chronic hepatitis B. Cancer Res 64(9):3326–3333
19. Okamoto M, Furuichi S, Nishioka Y, Oshikawa T, Tano T, Ahmed SU, Takeda K, Akira S, Ryoma Y, Moriya Y, Saito M, Sone S, Sato M (2004) Expression of toll-like receptor 4 on dendritic cells is significant for anticancer effect of dendritic cell-based immunotherapy in combination with an active component of OK-432, a streptococcal preparation. Cancer Res 64(15):5461–5470. doi:10.1158/0008-5472.CAN-03-4005
20. Hill KS, Errington F, Steele LP, Merrick A, Morgan R, Selby PJ, Georgopoulos NT, O'Donnell DM, Melcher AA (2008) OK432-activated human dendritic cells kill tumor cells via CD40/CD40 ligand interactions. J Immunol 181(5):3108–3115
21. Banchereau J, Steinman RM (1998) Dendritic cells and the control of immunity. Nature 392(6673):245–252. doi:10.1038/32588
22. Timmerman JM, Czerwinski DK, Davis TA, Hsu FJ, Benike C, Hao ZM, Taidi B, Rajapaksa R, Caspar CB, Okada CY, van Beckhoven A, Liles TM, Engleman EG, Levy R (2002) Idiotype-pulsed dendritic cell vaccination for B-cell lymphoma: clinical and immune responses in 35 patients. Blood 99(5):1517–1526
23. Banchereau J, Palucka AK, Dhodapkar M, Burkeholder S, Taquet N, Rolland A, Taquet S, Coquery S, Wittkowski KM, Bhardwaj N, Pineiro L, Steinman R, Fay J (2001) Immune and clinical responses in patients with metastatic melanoma to CD34(+) progenitor-derived dendritic cell vaccine. Cancer Res 61(17):6451–6458
24. Okada H, Kalinski P, Ueda R, Hoji A, Kohanbash G, Donegan TE, Mintz AH, Engh JA, Bartlett DL, Brown CK, Zeh H, Holtzman MP, Reinhart TA, Whiteside TL, Butterfield LH, Hamilton RL, Potter DM, Pollack IF, Salazar AM, Lieberman FS (2011) Induction of CD8 + T-cell responses against novel glioma-associated antigen peptides and clinical activity by vaccinations with {alpha}-type 1 polarized dendritic cells and polyinosinic-polycytidylic acid stabilized by lysine and carboxymethylcellulose in patients with recurrent malignant glioma. J Clin Oncol 29(3):330–336. doi:10.1200/JCO.2010.30.7744
25. Suso EM, Dueland S, Rasmussen AM, Vetrhus T, Aamdal S, Kvalheim G, Gaudernack G (2011) hTERT mRNA dendritic cell vaccination: complete response in a pancreatic cancer patient associated with response against several hTERT epitopes. Cancer Immunol Immunother 60(6):809–818. doi:10.1007/s00262-011-0991-9
26. Frey B, Weiss EM, Rubner Y, Wunderlich R, Ott OJ, Sauer R, Fietkau R, Gaipl US (2012) Old and new facts about hyperthermia-induced modulations of the immune system. Int J Hyperthermia 28(6):528–542. doi:10.3109/02656736.2012.677933
27. Rubner Y, Wunderlich R, Ruhle PF, Kulzer L, Werthmoller N, Frey B, Weiss EM, Keilholz L, Fietkau R, Gaipl US (2012) How does ionizing irradiation contribute to the induction of anti-tumor immunity? Front Oncol 2:75. doi:10.3389/fonc.2012.00075
28. den Brok MH, Sutmuller RP, van der Voort R, Bennink EJ, Figdor CG, Ruers TJ, Adema GJ (2004) In situ tumor ablation creates an antigen source for the generation of antitumor immunity. Cancer Res 64(11):4024–4029. doi:10.1158/0008-5472.CAN-03-3949
29. Forster R, Schubel A, Breitfeld D, Kremmer E, Renner-Muller I, Wolf E, Lipp M (1999) CCR7 coordinates the primary immune response by establishing functional microenvironments in secondary lymphoid organs. Cell 99(1):23–33
30. Ferlazzo G, Tsang ML, Moretta L, Melioli G, Steinman RM, Munz C (2002) Human dendritic cells activate resting natural killer (NK) cells and are recognized via the NKp30 receptor by activated NK cells. J Exp Med 195(3):343–351
31. Morandi B, Mortara L, Chiossone L, Accolla RS, Mingari MC, Moretta L, Moretta A, Ferlazzo G (2012) Dendritic cell editing by activated natural killer cells results in a more protective cancer-specific immune response. PLoS ONE 7(6):e39170. doi:10.1371/journal.pone.0039170

32. Ab BK, Kiessling R, Van Embden JD, Thole JE, Kumararatne DS, Pisa P, Wondimu A, Ottenhoff TH (1990) Induction of antigen-specific CD4+ HLA-DR-restricted cytotoxic T lymphocytes as well as nonspecific nonrestricted killer cells by the recombinant mycobacterial 65-kDa heat-shock protein. Eur J Immunol 20(2):369–377. doi:10.1002/eji.1830200221

33. Bourgault I, Gomez A, Gomard E, Picard F, Levy JP (1989) A virus-specific CD4+ cell-mediated cytolytic activity revealed by CD8+ cell elimination regularly develops in uncloned human antiviral cell lines. J Immunol 142(1):252–256

PLOS ONE

Ectopic Fat Accumulation and Distant Organ-Specific Insulin Resistance in Japanese People with Nonalcoholic Fatty Liver Disease

Ken-ichiro Kato[1☯], Toshinari Takamura[1*☯], Yumie Takeshita[1], Yasuji Ryu[2], Hirofumi Misu[1], Tsuguhito Ota[1], Kumpei Tokuyama[3], Shoichiro Nagasaka[4], Munehide Matsuhisa[5], Osamu Matsui[2], Shuichi Kaneko[1]

1 Department of Disease Control and Homeostasis, Kanazawa University Graduate School of Medical Sciences, Kanazawa, Ishikawa, Japan, **2** Department of Radiology, Kanazawa University Graduate School of Medical Sciences, Kanazawa, Ishikawa, Japan, **3** Graduate School of Comprehensive Human Science, University of Tsukuba, Tsukuba, Ibaraki, Japan, **4** Department of Medicine, Division of Endocrinology and Metabolism, Jichi Medical University, Shimono, Tochigi, Japan, **5** Clinical Research Center for Diabetes, Tokushima University, Tokushima, Tokushima, Japan

Abstract

Objective: The aim of this study was to examine the association between ectopic fat and organ-specific insulin resistance (IR) in insulin-target organs in patients with nonalcoholic fatty liver disease (NAFLD).

Methods: Organ-specific IR in the liver (hepatic glucose production (HGP)×fasting plasma insulin (FPI) and suppression of HGP by insulin [%HGP]), skeletal muscle (insulin-stimulated glucose disposal [Rd]), and adipose tissue (suppression of FFA by insulin [%FFA]) was measured in 69 patients with NAFLD using a euglycemic hyperinsulinemic clamp with tracer infusion ([6,6-$^2H_2$]glucose). Liver fat, intramyocellular lipid (IMCL), and body composition were measured by liver biopsy, proton magnetic resonance spectroscopy, and bioelectrical impedance analysis, respectively.

Results: HGP×FPI was significantly correlated with Rd ($r=-0.57$, $P<0.001$), %HGP with %FFA ($r=0.38$, $P<0.01$), and Rd with %FFA ($r=0.27$, $P<0.05$). Liver steatosis score was negatively associated with Rd ($r=-0.47$, $P<0.001$) as well as with HGP×FPI ($r=0.43$, $P<0.001$). Similarly, intrahepatic lipid was negatively associated with Rd ($r=-0.32$, $P<0.05$). IMCL was not associated with Rd ($r=-0.16$, $P=0.26$). Fat mass and its percentage were associated with HGP×FPI ($r=0.50$, $P<0.001$; $r=0.48$, $P<0.001$, respectively) and Rd ($r=-0.59$, $P<0.001$; $r=-0.52$, $P<0.001$, respectively), but not with %FFA ($r=-0.21$, $P=0.10$; $r=-0.001$, $P=0.99$, respectively).

Conclusion: Unexpectedly, fat accumulation in the skeletal muscle and adipose tissue was not associated with organ-specific IR. Instead, liver fat was associated not only with hepatic IR but also with skeletal muscle IR, suggesting a central role of fatty liver in systemic IR and that a network exists between liver and skeletal muscle.

Citation: Kato K-i, Takamura T, Takeshita Y, Ryu Y, Misu H, et al. (2014) Ectopic Fat Accumulation and Distant Organ-Specific Insulin Resistance in Japanese People with Nonalcoholic Fatty Liver Disease. PLoS ONE 9(3): e92170. doi:10.1371/journal.pone.0092170

Editor: Yanqiao Zhang, Northeast Ohio Medical University, United States of America

Received December 29, 2013; **Accepted** February 18, 2014; **Published** March 20, 2014

Funding: This work was supported in part by a grant-in-aid for Scientific Research (C-20591054 to TT) from the Ministry of Education, Culture, Sports, Science, and Technology, Japan. The funders had no role in study design, data collection and analysis, decision to publish, or preparation of the manuscript. No additional external funding received for this study.

Competing Interests: The authors have declared that no competing interests exist.

* E-mail: ttakamura@m-kanazawa.jp

☯ These authors contributed equally to this work.

Introduction

Insulin resistance (IR) is a core pathology of type 2 diabetes mellitus (T2DM), nonalcoholic fatty liver disease (NAFLD), and cardiovascular diseases [1–3]. The severity of IR may differ among the major insulin-target organs, the liver, skeletal muscle, and adipose tissue [4]. Accumulating evidence suggests that ectopic fat accumulation in insulin-target organs leads to development of IR in each organ by altering oxidative stress [5–7] and gene expression profiles [8,9]. Indeed, liver steatosis is associated with whole-body IR, independently of body mass index (BMI) [10].

Conversely, inter-organ network and organ-derived bioactive hormones such as adiponectin and selenoprotein P may play a role in the development of distant organ IR [11–13]. Therefore, to understand organ networks that sense excess energy and regulate insulin action, elucidating the association between fat accumulation and organ-specific IR among the liver, skeletal muscle, and adipose tissue is important, especially in humans. However, no previous studies have demonstrated the association among these organs comprehensively and simultaneously [14,15]. In addition, liver biopsy remains gold standard for diagnosis of NAFLD because it more accurately measures liver fat than proton

magnetic resonance spectroscopy (^{1}H-MRS) under some conditions [16].

The present study try to address the association of organ-specific IR with ectopic fat among the liver, skeletal muscle, and adipose tissue in Japanese patients with NAFLD, systematically using reliable methods including liver biopsy, assessment of glucose metabolism measured by a euglycemic hyperinsulinemic clamp study with stable-isotope, and ^{1}H-MRS.

Materials and Methods

Ethics Statement

The study was approved by the Medical Ethics Committee of Kanazawa University (Approval No. 845), and written informed consent was obtained from each patient prior to participation. The study was conducted in accordance with the Declaration of Helsinki.

Participants and Study Design

We studied 69 patients clinically diagnosed with NAFLD, recruited consecutively between 2010 and 2012 from Kanazawa University Hospital, Japan. The patients were in good general health without evidence of any acute or chronic diseases (other than NAFLD, T2DM, hypertension, or dyslipidemia) as determined by history, physical examination, routine blood chemistries, urinalysis, and electrocardiography. Out of the 69 patients, 37 (54%) had T2DM according to the American Diabetes Association criteria. Of the 37 T2DM patients, antidiabetic agents were administered to 18 patients in monotherapy and 7 patients in combination therapy (metformin, n = 15; dipeptidyl peptidase-4 inhibitors, n = 9; glucagon-like peptide-1 agonists, n = 7; mealtime dosing of a rapid-acting insulin analog, n = 5, respectively). None of the patients were taking α-glucosidase inhibitors, rapid-acting insulin secretion agents, sulfonylurea, thiazolidinediones, or long-acting insulin. Participants were excluded if they had a history of alcohol abuse (more than 20 g/day), liver diseases other than NAFLD (hepatitis B or C, autoimmune hepatitis, hemochromatosis, Wilson disease, drug-induced disease, or other), type 1 diabetes, or a history of clinically significant renal, pulmonary, or heart diseases.

The participants were studied on four separate occasions. Generally, all measurements were performed within 1 month and included: 1) organ-specific IR in the liver, skeletal muscle, and adipose tissue by a euglycemic hyperinsulinemic clamp study with tracer ([6,6-$^2H_2$]glucose) infusion; 2) liver biopsy for histology to confirm the diagnosis of NAFLD and score the degree of steatosis, grade, and stage; 3) intrahepatic lipid (IHL) and intramyocellular lipid (IMCL) measured by ^{1}H-MRS, and body composition by a bioelectrical impedance analysis; and 4) 75-g oral glucose tolerance test (OGTT) to evaluate the glucose tolerance according to American Diabetes Association criteria [17].

Euglycemic Hyperinsulinemic Clamp

After an overnight fast, two intravenous catheters, one for blood sampling and one for infusion of glucose, insulin, and tracers, were inserted in the antecubital vein of each arm. At 0700 h, after obtaining a blood sample for background enrichment of plasma glucose, a continuous infusion of [6,6-$^2H_2$]glucose (>99% enriched; Cambridge Isotope, Andover, MA, USA) was started at a rate of 0.05 mg·kg^{-1}·min^{-1} after a priming dose equivalent. After 100, 110, and 120 min, blood samples were obtained for determination of tracer enrichments. Subsequently, at 0900 h, the euglycemic hyperinsulinemic clamp study was started using an artificial pancreas (model STG-55; Nikkiso, Tokyo, Japan), as described previously [18,19]. A primed continuous infusion of insulin (Humulin R; Eli Lilly, Indianapolis, IN, USA) was started for 2.0 h at a rate of 1.25 mU·kg^{-1}·min^{-1} to attain a plasma insulin concentration of approximately 100 μU/mL. Glucose was infused to maintain a plasma glucose concentration of 100 mg/dL (or 90 mg/dL for baseline values under 90 mg/dL). Simultaneously, [6,6-$^2H_2$]glucose infusion was continued at a rate of 0.15 mg·kg^{-1}·min^{-1}. During the last 20 min of the clamp study, blood samples were obtained in 10-min intervals to determine tracer enrichments.

Liver Biopsy/Pathology

Ultrasound-guided liver biopsy specimens were obtained from all 69 patients. Each specimen was stained with hematoxylin-eosin and silver reticulin stains and histologically examined by one experienced pathologist who was blinded to the patient's clinical condition and biochemical data. The biopsied tissues were scored for steatosis (0, none; 1, <33%; 2, 33–66%; 3, >66%), stage, and grade as described previously (10), according to the standard criteria for grading and staging of nonalcoholic steatohepatitis proposed by Brunt et al. [20,21].

Liver Fat Content and IMCL (Proton Magnetic Resonance Spectroscopy)

IHL and IMCL were measured as reported previously [22,23]. Briefly, IHL of the liver's right lobe and IMCL of the soleus muscle were measured by ^{1}H-MRS using a whole-body 3.0 T MR System (Signa HDxt 3.0 T, General Electric Healthcare, Milwaukee, WI, USA). Voxels (3.0×3.0×3.0 cm^3 for liver and 2.0×2.0×2.0 cm^3 for soleus muscle) were positioned in the liver or soleus muscle to avoid blood vessels and visible interfacial fat, and the voxel sites were carefully matched at each examination. Imaging parameters were set to repetition time of 1500 ms and echo time of 27 ms. To quantify IHL and IMCL, the MR spectral raw data were processed by using the LCModel software (Version 6.3-0C, Stephen Provencher, Oakville, Ontario, Canada).

Body Composition

Body composition, such as fat mass and fat-free mass, was determined by a bioelectrical impedance analysis (Tanita BC-118D, Tanita, Tokyo, Japan).

Oxygen Consumption

Oxygen consumption was measured using indirect calorimetry (Aeromonitor AE310S, Minato, Osaka, Japan).

75-g OGTT

After an overnight fast, a 75-g OGTT was performed at 0800 h. Blood samples were collected at 0, 30, 60, 90, 120, and 180 min to measure plasma glucose insulin and C-peptide concentrations.

Analytical Methods

Plasma glucose was measured by the glucose oxidase method (Glucose Analyzer GA09; A&T, Kanagawa, Japan), and plasma insulin and C-peptide were measured using a sandwich enzyme immunoassay system with E-test Tosoh II (IRI) and E-test Tosoh II (C-peptide) (Tosoh, Tokyo, Japan). Plasma FFA was measured by a standard colorimetric method using NEFA-SS (Eiken, Tokyo, Japan). Hemoglobin A1c level was measured using high-performance liquid chromatography (TOSOH HLC-723G8; Tosoh, Tokyo, Japan).

Deuterated glucose was analyzed as a penta-acetate derivative using the method by Wolfe [24]. Samples were analyzed on a

quadrupole gas chromatography mass spectrometry instrument (GCMS-QP1100EX, Shimadzu, Kyoto, Japan) operated in the electron impact mode by selective-ion monitoring of m/z 200, 201, and 202. Oven temperature was 180°C with a 10°C/min rate of temperature rise until 250°C with a 25 m HR-1 capillary column (Shinwa Chemical Industries, Kyoto, Japan). Tracer concentrations were calculated based on the sample's tracer-to-tracee mass ratio [25].

Calculations

In the basal state, hepatic glucose production (HGP) was calculated as the rate of appearance (Ra) of glucose according to the Steele's equation as previously described [19,26]. During the clamp study, glucose Ra was calculated using Steele's equation from tracer data [26]. HGP during the clamp study was calculated as the difference between glucose Ra and the infusion rate of exogenous glucose.

We calculated and defined organ-specific IR in the liver, skeletal muscle, and adipose tissue as described previously [27–30]. Hepatic IR indices were calculated as the product of fasting HGP and fasting plasma insulin (FPI) concentration (HGP×FPI [$(mg \cdot kg^{-1} \cdot min^{-1}) \times (\mu U/mL)$]) and suppression of HGP by insulin during a clamp study (%HGP). The skeletal muscle IR index was calculated as insulin-stimulated glucose disposal (Rd), and the adipose tissue IR index was calculated as suppression of FFA by insulin during a clamp study (%FFA).

Statistical Analysis

All analyses were performed using SPSS software version 21.0 (SPSS Inc., Chicago, IL, USA). All values are expressed as mean ± SEM, unless stated otherwise. The relationship between individual variables was assessed by Pearson's correlation for parametric variables and by Spearman's correlation for non-parametric variables. Multiple linear regression analysis was used to assess independent determinants of organ-specific IR. The differences between the two groups were assessed by Student's *t*-test for continuous variables and chi-square test for categorical variables. Data involving more than two groups were assessed by analysis of variance (ANOVA). Statistical significance was considered to be $P<0.05$.

Results

Organ-specific IR and Clinical Characteristics in Patients with NAFLD

The characteristics of the study subjects and their metabolic profiles are shown in Table 1. During the clamp study, plasma glucose concentrations were maintained at baseline values (103±1 mg/dL; mean ± SEM), and steady-state plasma insulin concentrations were reached at 110.2±3.6 μU/mL. Basal HGP was 2.09±0.08 $mg \cdot kg^{-1} \cdot min^{-1}$ in subjects with normal glucose tolerance (NGT), 2.18±0.10 $mg \cdot kg^{-1} \cdot min^{-1}$ in subjects with impaired glucose tolerance (IGT) and 2.67±0.12 $mg \cdot kg^{-1} \cdot min^{-1}$ in subjects with T2DM. Rd was 3.81±0.18 $mg \cdot kg^{-1} \cdot min^{-1}$ in NGT, 3.27±0.17 $mg \cdot kg^{-1} \cdot min^{-1}$ in IGT and 3.57±0.14 $mg \cdot kg^{-1} \cdot min^{-1}$ in T2DM. Basal FFA was 0.47±0.05 mEq/L in NGT, 0.56±0.04 mEq/L in IGT and 0.60±0.04 mEq/L in T2DM. Basal HGP showed a significant positive correlation with fasting plasma glucose levels ($r=0.48$, $P<0.001$). Rd showed a significant positive correlation with basal oxygen consumption rate per body weight (VO_2) ($r=0.42$, $P<0.01$). FFA and HGP were suppressed from baseline by 77.0±1.4% and 69.3±2.8%, respectively. These values are similar to previous data in Japanese [31] and European descent [1,27,29] subjects.

The relationship between clinical characteristics and organ-specific insulin sensitivity/resistance indices is shown in Table 2. HGP×FPI was significantly correlated with Rd ($r=-0.57$, $P<0.001$), %HGP with %FFA ($r=0.38$, $P<0.01$), and Rd with %FFA ($r=0.27$, $P<0.05$) suggesting that the IRs in the liver, skeletal muscle, and adipose tissue were significantly associated with each other, although the correlation was not very strong.

Ectopic Fat and Organ-specific IR

Histological liver steatosis score was strongly correlated with IHL measured by ^{1}H-MRS ($r=0.75$, $P<0.001$).

Liver steatosis score was significantly correlated with Rd ($r=-0.47$, $P<0.001$) as well as HGP×FPI ($r=0.43$, $P<0.001$) (Table 2). Similarly, IHL was significantly correlated with Rd ($r=-0.32$, $P<0.05$) and tended to be correlated with HGP×FPI ($r=0.25$, $P=0.09$) (Figure 1A, 1B). In the multiple regression analysis, liver steatosis score was significantly correlated with both HGP×FPI ($\beta=0.284$, $P<0.05$) and Rd ($\beta=-0.300$, $P<0.01$) after adjusting for age, sex, and BMI. Correlation of liver steatosis score with Rd ($\beta=-0.261$, $P<0.05$) was significant after further adjusting for total fat mass (Table 3). When stratified by steatosis score, HGP×FPI was significantly higher and Rd was significantly lower in the score 3 steatosis group compared to the score 0 steatosis group ($P<0.01$; $P<0.001$, respectively) (Figure 1C,1D).

Unexpectedly, indices of fat accumulation in the skeletal muscle (IMCL) and adipose tissue were not associated with their own organ-specific IR (Table 2). IMCL and fat-free mass were not correlated with Rd ($r=-0.16$, $P=0.26$; $r=-0.22$, $P=0.08$, respectively) (Figure 2A,2B). Total fat mass and its percentage were correlated with HGP×FPI ($r=0.50$, $P<0.001$; $r=0.48$, $P<0.001$, respectively) and Rd ($r=-0.59$, $P<0.001$; $r=-0.52$, $P<0.001$, respectively), but not with %FFA ($r=-0.21$, $P=0.10$; $r=-0.00$, $P=0.99$, respectively) (Figure 2C,2D).

Similar results were obtained when Rd was normalized by steady state plasma insulin (Rd/SSPI) (Table 2).

Because it may be possible that T2DM itself is associated with IR independently with organ steatosis, we analyzed the subjects with or without T2DM. Age, hemoglobin A1c, fasting plasma glucose, 2-h glucose level of 75-g OGTT and basal HGP were significantly higher in T2DM group compared to non-DM group (Table 1). Regardless of the presence or absence of T2DM, liver steatosis score was significantly correlated with Rd as well as HGP×FPI, and IMCL and total fat mass were not correlated with Rd or %FFA respectively (Table 4, Table 5). The results of the multiple regression analysis are shown in Table S1 and Table S2.

Discussion

We comprehensively and simultaneously evaluated ectopic fat accumulation and organ-specific IR in insulin-target organs in Japanese people with NAFLD, and found the following: 1) the IRs in the liver, skeletal muscle, and adipose tissue were associated with each other, 2) indices of fat accumulation in the skeletal muscle and adipose tissue were not associated with their own organ-specific IR, and 3) liver fat was associated with skeletal muscle IR as well as hepatic IR, independently of age, sex, BMI and total fat mass (Figure S1).

Although the IRs in the liver, skeletal muscle, and adipose tissue were associated with each other, the relation was relatively weak. There are a couple possible explanations for this result. First, the main site and the severity of IR may vary among organs and individuals [4]. Second, possibly the %HGP and %FFA are not

Table 1. Clinical characteristics of the study subjects.

	All	non-DM (NGT+IGT)	T2DM	*P* value*
n	69	32	37	
Age (years)	51±2	46±3	55±2	0.008[b]
Sex (Male/Female)	42/27	23/9	19/18	0.082
Body mass index (kg/m^2)	30.3±0.9	30.9±1.2	29.8±1.4	0.526
Weight (kg)	82.3±2.7	86.5±3.8	78.6±3.9	0.152
Fat-free mass (kg)	50.2±1.3	52.7±1.6	47.9±1.9	0.058
Total fat mass (kg)	30.6±2.0	31.0±2.9	30.2±2.9	0.855
Body fat percentage (%)	36.3±1.3	35.6±1.9	37.0±1.8	0.594
Historogical scores				
Steatosis (0/1/2/3)	5/33/15/16	4/13/5/10	1/20/10/6	
Grade (0/1/2/3)	15/35/16/3	10/14/7/1	5/21/9/2	
Stage (0/1/2/3/4)	20/29/6/11/3	12/14/1/4/1	8/15/5/7/2	
NAFLD activity score (0/1/2/3/4/5/6/7/8)	3/5/12/14/12/9/13/1/0	2/4/4/7/4/5/5/1/0	1/1/8/7/8/4/8/0/0	
IHL (mmol/L)	9.63±1.01	7.30±1.27	11.23±1.41	0.056
IMCL (AU, ratio relative to creatine)	28.29±1.49	27.91±2.21	28.58±2.04	0.827
Glucose tolerance (NGT/IGT/DM)	11/21/37			
Hemoglobin A1C (%)	6.5±0.1	6.0±0.1	7.0±0.1	<0.001[c]
Fasting plasma glucose (mg/dL)	111±2	100±2	121±3	<0.001[c]
2-h glucose (mg/dL)	208±10	142±6	265±12	<0.001[c]
Fasting plasma insulin (μU/mL)	14.0±1.0	15.1±1.5	13.1±1.3	0.318
2-h insulin (μU/mL)	139.1±12.6	157.2±21.8	123.5±13.7	0.182
Insulinogenic index [(μU/mL)/(mg/dL)]	0.72±0.09	0.95±0.16	0.52±0.09	0.019[a]
Fasting C-peptide (ng/mL)	2.9±0.1	3.1±0.2	2.7±0.2	0.199
Fasting FFAs (mEq/L)	0.57±0.03	0.53±0.03	0.60±0.04	0.254
Total cholesterol (mg/dL)	176±4	185±6	169±6	0.061
Triglycerides (mg/dL)	153±11	150±10	155±18	0.801
HDL cholesterol (mg/dL)	41±1	41±2	41±2	0.927
Aspartate aminotransferase (IU/L)	37±2	37±3	37±3	0.969
Alanine aminotransferase (IU/L)	60±4	62±6	59±5	0.752
Basal HGP (mg·kg^{-1}·min^{-1})	2.43±0.08	2.15±0.07	2.67±0.12	0.001[b]
HGP×FPI [(mg·kg^{-1}·min^{-1})×(μU/mL)]	32.0±2.0	31.2±2.8	32.7±2.9	0.707
Euglycemic hyperinsulinemic clamp [clamp period]				
Clamped glucose (mg/dL)	103±1	102±2	104±2	0.592
Steady state plasma insulin (μU/mL)	110.2±3.6	115.7±6.0	105.3±4.2	0.164
FFAs (mEq/L)	0.13±0.01	0.13±0.01	0.13±0.01	0.884
%FFA (%)	77.0±1.4	75.9±2.0	78.0±1.9	0.455
HGP (mg·kg^{-1}·min^{-1})	0.69±0.07	0.56±0.07	0.81±0.12	0.088
%HGP (%)	69.3±2.8	73.4±3.5	65.8±4.1	0.170
Rd (mg·kg^{-1}·min^{-1})	3.52±0.10	3.45±0.14	3.57±0.14	0.556
Rd/SSPI [(mg·kg^{-1}·min^{-1})/(μU/mL)]	0.035±0.002	0.033±0.003	0.037±0.003	0.332
VO_2 (ml·kg^{-1}·min^{-1})	2.85±0.04	2.84±0.07	2.86±0.06	0.817

Data are presented as n or mean ± SEM.
IHL, intrahepatic lipid; IMCL, intramyocellular lipid; AU, arbitrary units; HGP, hepatic glucose production; FPI, fasting plasma insulin; SSPI, steady state plasma insulin; VO_2, basal oxygen consumption rate per body weight.
*Difference between the non-DM group and the T2DM group.
[a]$P<0.05$,
[b]$P<0.01$,
[c]$P<0.001$.
doi:10.1371/journal.pone.0092170.t001

completely suitable for indices of hepatic and adipose tissue IR, respectively, and might not fully exhibit inter-individual variation because HGP and lipolysis appeared to be more sensitive to suppression by insulin compared to stimulation of Rd by insulin

Table 2. Univariate correlation between ectopic fat and organ-specific insulin resistance.

	HGP×FPI		%HGP		Rd		Rd/SSPI		%FFA	
	r	*P*	*r*	*P*	*r*	*P*	*r*	*P*	*r*	*P*
HGP×FPI	1	–	−0.130	0.288	−0.574[c]	<0.001	−0.489[c]	<0.001	−0.168	0.167
%HGP	−0.130	0.288	1	–	0.167	0.170	0.387[b]	0.001	0.375[b]	0.002
Rd	−0.574[c]	<0.001	0.167	0.170	1	–	0.766[c]	<0.001	0.272[a]	0.024
Rd/SSPI	−0.489[c]	<0.001	0.387[b]	0.001	0.766[c]	<0.001	1	–	0.296[a]	0.014
%FFA	−0.168	0.167	0.375[b]	0.002	0.272[a]	0.024	0.296[a]	0.014	1	–
Steatosis	0.428[c]	<0.001	−0.148	0.226	−0.473[c]	<0.001	−0.430[c]	<0.001	−0.121	0.322
Grade	0.338[b]	0.004	−0.111	0.362	−0.376[b]	0.001	−0.338[b]	0.005	−0.055	0.656
Stage	0.283[a]	0.019	−0.098	0.422	−0.348[b]	0.003	−0.261[a]	0.031	−0.010	0.933
IHL	0.245	0.089	−0.114	0.436	−0.315[a]	0.028	−0.271	0.062	−0.135	0.356
IMCL	0.250	0.065	−0.215	0.115	−0.156	0.256	−0.183	0.185	−0.060	0.662
Fat-free mass	0.031	0.801	−0.117	0.347	−0.216	0.079	−0.211	0.090	−0.433[c]	<0.001
Total fat mass	0.495[c]	<0.001	−0.147	0.235	−0.594[c]	<0.001	−0.536[c]	<0.001	−0.205	0.096
Body fat percentage	0.481[c]	<0.001	−0.115	0.355	−0.518[c]	<0.001	−0.478[c]	<0.001	−0.001	0.994
VO_2	−0.129	0.342	0.191	0.158	0.418[b]	0.001	0.405[b]	0.002	0.115	0.397

HGP, hepatic glucose production; FPI, fasting plasma insulin; SSPI, steady state plasma insulin; IHL, intrahepatic lipid; IMCL, intramyocellular lipid; VO_2, basal oxygen consumption rate per body weight.
[a]$P<0.05$,
[b]$P<0.01$,
[c]$P<0.001$.
doi:10.1371/journal.pone.0092170.t002